cmgh
CELLULAR AND MOLECULAR GASTROENTEROLOGY AND HEPATOLOGY

ORIGINAL RESEARCH

# Hyperactive Enteric Glia Contribute to Persistent Dysmotility Following Inflammation by Driving Aberrant Excitatory Responses in Neurons

Luisa Seguella,[1,2,*] Beatriz Thomasi,[1,*] Silvia Basili Franzin,[2] Jonathon L. McClain,[1] Rafaella Lavalle,[1] Aurora Zilli,[1,2] Visha Parmar,[1] Giuseppe Esposito,[2] and Brian D. Gulbransen[1]

[1]*Department of Physiology, Michigan State University, East Lansing, Michigan; and* [2]*Department of Physiology and Pharmacology "V. Erspamer", Sapienza University of Rome, Rome, Italy*

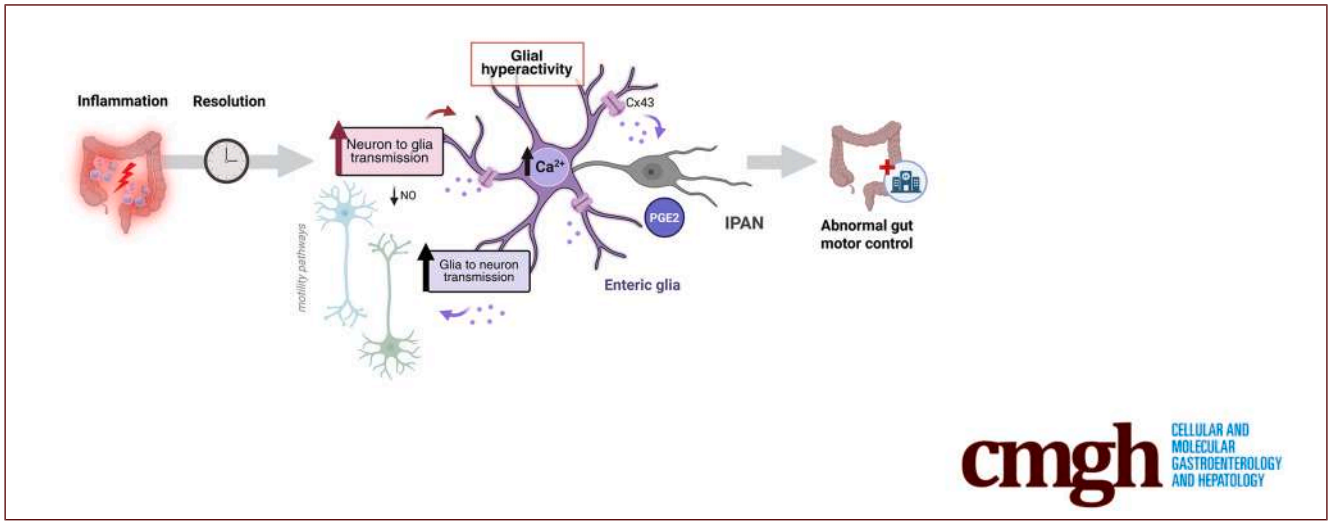


## SUMMARY

This study shows that "hyperactive" enteric glia contribute to mechanisms that drive long-lasting changes in gut motility following an acute bout of inflammation through abnormal neuron-to-glia and glia-to-neuron communication.

**BACKGROUND & AIMS:** Experiencing gut inflammation often produces long-term defects in gut motor function that persist despite the resolution of active inflammation. Such changes are driven by neuroplasticity within enteric nervous system motor neurocircuits and contribute to the pathophysiology of common disorders that include postinfectious irritable bowel syndrome and inflammatory bowel disease in remission. Yet mechanisms that drive and maintain enteric neuroplasticity following inflammation are poorly understood.

**METHODS:** We studied cellular activity in enteric motor neurocircuits and gut motor function following the resolution of acute inflammation using genetically encoded $Ca^{2+}$ sensors and chemogenetics to test the hypothesis that acute inflammation induces glial changes that promote neuron hyperexcitability with subsequent effects on gut motor functions.

**RESULTS:** The data show that enteric glia are hyperexcitable following acute inflammation and drive abnormal excitatory responses in enteric neurons that disrupt gut motor control. Enteric neurons in synaptically connected neural pathways are more excitable following colitis and stimulate greater activity among the surrounding enteric glia. Chemogenetic activation experiments show that enteric glia exhibit intrinsic hyperexcitability and that subsequent gliotransmission mechanisms trigger abnormal responses in neurons that alter motor responses. Mechanisms underlying glial hyperexcitability involve changes to nitrergic inhibition, prostaglandin $E_2$, and enhanced glial connexin-43 hemichannel activity.

**CONCLUSIONS:** These observations suggest that therapies targeting enteric glial signaling mechanisms could aid persistent gut dysmotility caused by inflammation. *(Cell Mol Gastroenterol Hepatol 2026;20:101634; https://doi.org/10.1016/j.jcmgh.2025.101634)*

*Keywords:* Autonomic; Enteric Nervous System; Gut; Intestine; Neuroinflammation.

Changes in colonic motility often manifest as symptoms that include constipation, diarrhea, and pain, which are each among the top reasons that individuals seek

medical care.[1] Symptoms of colonic dysmotility can be debilitating, socially restrictive, and difficult to treat. This is particularly relevant for individuals with disorders of gut-brain interaction (DGBI) such as irritable bowel syndrome (IBS) and organic gastrointestinal diseases such as inflammatory bowel diseases (IBD) in which colon dysmotility is common in active disease and during remission.[2,3] A major current hypothesis explaining the emergence of colon dysmotility in IBS and its persistence in IBD during remission is that experiencing gut inflammation imparts long-lasting effects on gut motor function.[4,5] Many new cases of IBS arise following acute gut inflammation,[6] and repeated bouts of inflammation in active IBD cause persistent gut dysfunction during clinical remission to produce a condition loosely termed IBS-IBD.[7–9] It is now generally accepted that experiencing an acute bout of gastroenteritis is a prominent risk factor for developing long-term gut dysfunction; however, the cellular targets and mechanisms responsible for maintaining the effects of inflammation on gut motility remain poorly understood.

Motor behaviors of the intestine are controlled by the enteric nervous system (ENS). The ENS is a large, integrative neural network that is housed entirely within the walls of the intestine and composed of enteric sensory neurons (intrinsic primary afferent neurons [IPANs]), excitatory and inhibitory motor neurons, interneurons, and glia.[10] Inflammation imparts long-lasting changes to the ENS that disrupt functional connectivity of enteric neurocircuits, neuromuscular communication, and ultimately, intestinal motility. Multiple neuroplastic changes occur in the ENS following inflammation including hyperexcitability among IPANs,[11–14] synaptic facilitation among interneurons,[15,16] defects in purinergic neuromuscular transmission,[17] inhibitory neuron death,[18,19] and reactive gliosis.[20] Yet mechanisms responsible for driving and maintaining abnormal enteric circuit activity remain poorly understood. Effects of inflammation could be directly imprinted on neurons; however, it is equally possible that inflammation-driven changes to enteric neural circuits involve indirect effects on neurons mediated by the surrounding glia.

Enteric glia are a unique type of peripheral neuroglia that accompany enteric neurons in the gut and maintain homeostasis in enteric neurocircuits.[20] Ongoing bidirectional communication between enteric glia and neurons refines the strength and specificity of signals that travel through enteric neural networks and control essential gut functions such as motility. Circuit-specific glia are devoted to distinct neural pathways that regulate motility,[20,21] and glia signaling exerts control over motility neurocircuits through actions on specific subsets of enteric neurons.[22–24] Enteric glia exhibit profound phenotypic changes in response to inflammation and promote neuroinflammation within the ENS.[25–29] The so-called "reactive" glial responses to inflammation produce acute effects that change the sensitivity of intrinsic and extrinsic sensory neurons innervating the gut and drive cell death among nitrergic inhibitory motor neurons in the ENS.[21,23,26] Yet how changes to glia might sustain the effects of inflammation on neuron activity within motility neurocircuits to promote abnormal motility is unknown.

Here, we studied cellular activity in enteric motor neurocircuits using genetically encoded $Ca^{2+}$ sensors following the resolution of acute inflammation and perturbed glial activity using chemogenetics to test the hypothesis that acute inflammation induces changes in enteric glia that promote persistent hyperexcitability in neurons and alter gut motor functions. The data show that enteric glia are hyperexcitable following colitis and drive abnormal excitatory responses in neurons that produce exaggerated motor responses. Mechanisms underlying glial hyperexcitability involve changes to nitrergic inhibitory tone, prostaglandin E2 ($PGE_2$) signaling, and enhanced glial connexin-43 hemichannel activity. These observations uncover a new mechanism of inflammatory-induced neuroplasticity in the gut and suggest that therapies targeting enteric glia could benefit intestinal motility disorders.

## Results

### *Acute Colitis Produces Postinflammatory Dysmotility*

Experiencing acute intestinal inflammation produces long-lasting changes in myenteric neurocircuitry that disrupt neural control of motility.[27,28] Enteric neuroplasticity induced by inflammation has been mostly characterized using the tri- or 2,4-di-nitrobenzene sulfonic acid (TNBS/DNBS) models of acute colitis due to their translational relevance, reproducibility, and ability to study both acute and chronic phases of inflammation-driven neuroplasticity, which includes myenteric neuron death,[18,19] synaptic facilitation,[15,16] and neuronal hyperexcitability.[11–13] Inflammation in the DNBS mouse model of acute colitis peaks between days 2 and 3 and resolves by day 7 (Figure 1*A*). As expected, mice challenged with DNBS lost body weight (Figure 1*B*), exhibited increased disease activity (Figure 1*C*), and showed clear evidence of histological tissue damage (Figure 1*D–F*) that peaked at day 2 and largely

*Authors share co-first authorship.

***Abbreviations used in this paper:*** **aFTS, ascending focal tract stimulation; ANOVA, analysis of variance; cFTS, circumferential focal tract stimulation; cGMP, cyclic guanosine 3′,5′-monophosphate; CMC, colonic motor complex; CMMP, circular muscle myenteric plexus; CNO, clozapine-N-oxide; CNS, central nervous system; Cx43, connexin-43; dFTS, descending focal tract stimulation; DGBI, disorders of gut-brain interaction; DMEM, Dulbecco's Modified Eagle Medium; DNBS, 2,4-di-nitrobenzene sulfonic acid; DREADD, designer receptor exclusively activated by designer drug; ENS, enteric nervous system; EtBr, ethidium bromide; FOV, field of view; FTS, focal tract stimulation; H&E, hematoxylin and eosin; IBD, inflammatory bowel diseases; IBS, irritable bowel syndrome; IHC, immunohistochemistry; IL, interleukin; IPAN, intrinsic primary afferent neuron; LMMP, longitudinal muscle myenteric plexus; PAPA NONOate, propylamine propylamine NONOate; PBS, phosphate buffered saline; PFA, paraformaldehyde; $PGE_2$, prostaglandin E2; ROI, region of interest; SD, standard deviation; SEM, standard error of the mean; tdT, tdTomato.**

**Most current article**



2352-345X
https://doi.org/10.1016/j.jcmgh.2025.101634

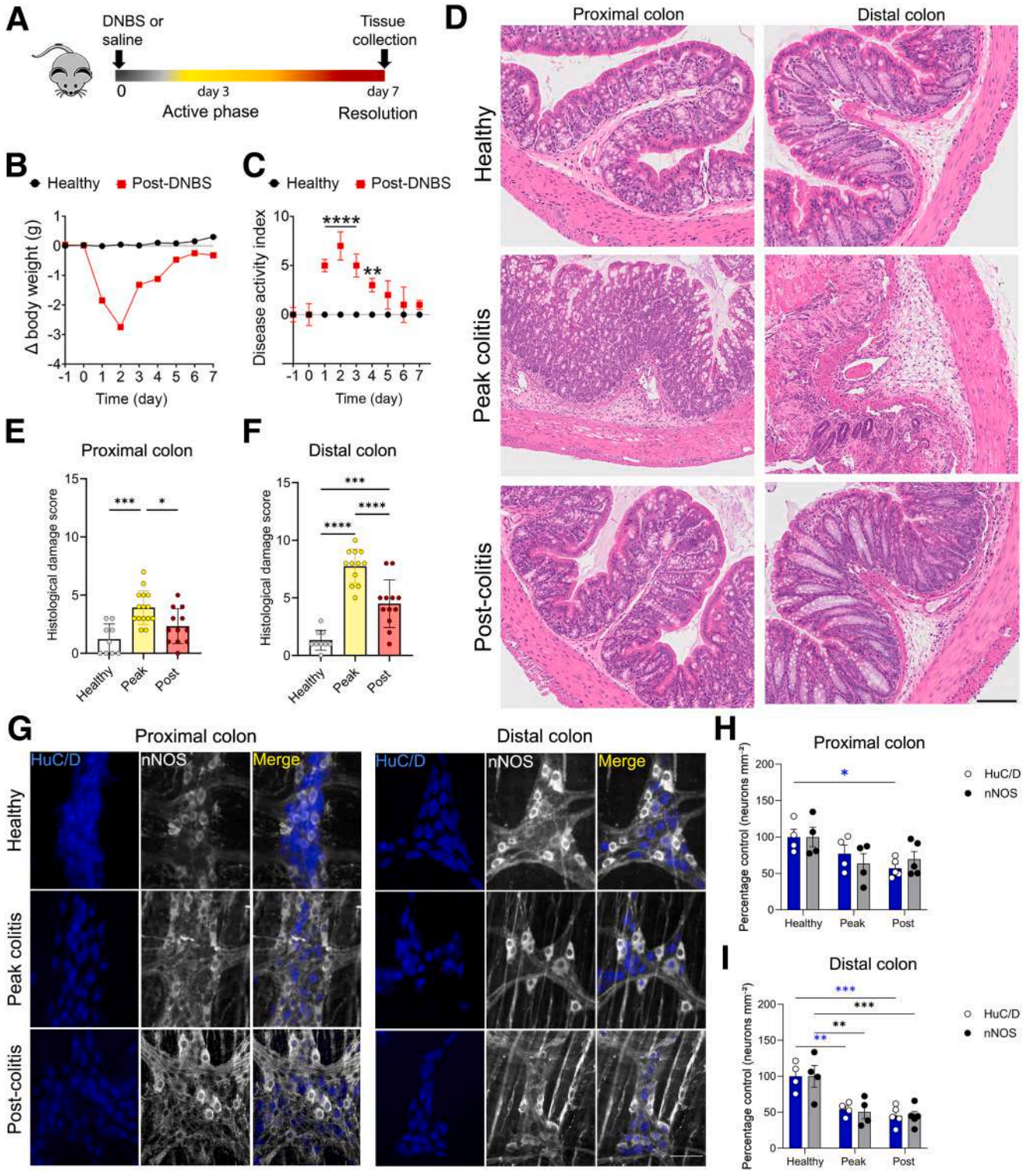


**Figure 1. Manifestation of disease activity and pathological hallmarks in the DNBS model of acute colitis.** (*A*) Diagram showing the timeline of acute DNBS colitis in mice. Active inflammation peaks around 48 to 72 hours and resolves within 7 days as reflected by changes in body weight (*B*) and disease activity index (*C*). Two-way ANOVA with Šídák's multiple comparisons test, $^{**}P < .01$, $^{****}P < .0001$; n = 5–6/group. Representative photomicrographs in healthy, peak of colitis and post-colitis (lines) in proximal and distal colon (columns). (*D–F*) Histological damage scores displayed in both colon regions throughout DNBS-induced colitis timeline. One-way ANOVA with Tukey's multiple comparison test, $^{*}P < .05$, $^{***}P < .001$, $^{****}P < .000$; n = 4-5. (*G*) Immunolabeling against HuC/D and nNOS in the myenteric plexus from healthy, peak colitis and post-DNBS mice and quantification of relative mean neuronal packing density in the proximal (*H*) and distal colon (*I*) myenteric plexus corrected by HuC/D and nNOS neuronal density in healthy tissues. Two-way ANOVA with Šídák's multiple comparisons test, $^{*}P < .05$, $^{**}P < .01$, $^{***}P < .001$; n = 4–5.

subsided by day 7. These animals also exhibited myenteric neurodegeneration that included a loss of nitrergic neurons in the distal colon (Figure 1*G–I*). These observations are consistent with prior studies that showed normalization of macroscopic and proinflammatory parameters as mice enter the post-inflammatory resolution phase around day 7 post-colitis,[18,19,21,23,26] and that neuroplastic effects such as neurodegeneration are still evident at this time. Likewise, evidence of tissue remodeling was still present in the distal colon at 7 days post-DNBS and likely reflects the greater damage induced at the initial site of injury and/or ongoing microscopic inflammation as observed in IBS and IBD in remission.[29,30]

Despite the apparent resolution of overt inflammation, motor defects were detected in animals that experienced colitis. Colonic motor complexes (CMCs) are a rhythmic pattern of colonic motor activity that is entirely under ENS command and persists in isolated organs ex vivo. Spontaneous CMCs typically generate in proximal regions of the colon and propagate in an oral to aboral direction via polarized enteric neurocircuitry.[31] Recordings of CMC activity in colons from healthy control animals and animals that experienced a prior bout of colitis (Figure 2*A*) showed that spontaneous CMCs arising from the oral side were similar in amplitude but were longer in duration (Figure 2*B*) and occurred less frequently (Figure 2*D*). Aboral recording sites showed that experiencing inflammation increased CMC amplitude in the distal colon (Figure 2*C*), caused a pronounced increase in their duration (Figure 2*C*), and decreased CMC propagation velocity (Figure 2*E*). These effects are consistent with those observed in prior work[13,19,32] and show that experiencing an acute bout of intestinal inflammation causes persistent functional changes that alter the neural control of gut motor function.

## Abnormal Myenteric Neurocircuit Activity in the Postinflammatory Gut

Neurocircuitry underlying gut motility consists of enteric sensory (IPAN), motor, and interneurons organized in synaptically connected ascending and descending neural pathways.[10] Prior electrophysiological studies showed that inflammation-induced enteric neuroplasticity involves changes to the properties of individual cell types in these circuits that include IPAN hyperexcitability and synaptic facilitation between interneurons and motor neurons.[11,33] How these and other cellular level changes affect functional enteric circuits that involve large cohorts of enteric neurons and glia remain unknown. We conducted $Ca^{2+}$ imaging experiments in samples from the distal and proximal colon of *Wnt1*$^{Cre2;GCaMP5g\text{-}tdT}$*;GFAP-hM3Dq* mice to understand how experiencing acute colitis affects gut motor neurocircuitry. This model allows simultaneous imaging of neuron and glial activity with the genetically encoded $Ca^{2+}$ indicator GCaMP5g, while also controlling glial activity through the clozapine-N-oxide (CNO)-induced activation of the glial-restricted Gq-coupled designer receptor exclusively activated by designer drug (DREADD) receptor hM3Dq (Figure 3*A*).[34] Enteric neurons and glia are easily differentiated in these experiments based on their distinct morphologies and expression of tdTomato (tdT), which is high in glia and low in neurons (Figure 3*B and C*),[34,35] likely due to differing mechanisms by which the tdTomato protein is handled in the two cell types.[36–38] We used this model to study neuron-to-glia communication by evoking neural activity with electrical stimulation of nerve fiber tracts (focal tract stimulation [FTS]) (Figure 3*D*) and used chemogenetic activation of glia to study the reciprocal effects of glia-to-neuron communication, also known as gliotransmission, on neurons (Figure 3*E*).

We began by assessing how experiencing inflammation changes neuronal activity in myenteric neurocircuits. FTS at sites oral or aboral to the ganglion of interest activates descending ("dFTS"; Figure 4*A*) or ascending ("aFTS"; Figure 4*F*) neural pathways, respectively, that project in opposite directions through the ganglion. These circuits are dominated by excitatory interneurons that synapse onto either excitatory or inhibitory motor neurons to produce contraction in the oral direction and distal relaxation. In addition, myenteric IPANs are multipolar cells that are synaptically connected to descending and ascending pathways and exhibit extensive projections oriented in the circumferential direction.[39,40] These neurons can be preferentially activated by stimulating circumferentially oriented fiber tracts (circumferential tract stimulation, "cFTS"; Figure 5*A*). Thus, we activated the distinct, overlapping neural pathways that course through ganglia by orientating an electrode in oral, aboral, or circumferential directions and assessed how inflammation impacts neurotransmission in these circuits.

In the proximal colon, mice that experienced inflammation exhibited larger amplitude neuronal $Ca^{2+}$ responses in cells functionally linked to descending (Figure 4*B–D*), ascending (Figure 4*G–I*), and circumferential pathways (Figure 5*B–D*). Similar amplifications of neuron responses were observed following inflammation in the distal colon; however, these were more robust in neurons associated with ascending pathways (Figure 4*G–I*) and circumferential pathways (Figure 5*B–D*) than in descending circuits (Figure 4*B–D*). The increase in neuron response amplitudes was not associated with changes in the numbers of responding neurons in ascending and descending pathways (Figure 4*E and J*), whereas a 19% increase in the number of neurons responding to cFTS was observed in the distal colon (Figure 5*E*).

Stratifying the data by sex revealed that the effects of inflammation on myenteric neural circuits are sexually dimorphic (Table 1). In general, neuron $Ca^{2+}$ response magnitudes were increased in both females and males in the proximal colon following inflammation, but numbers of responding neurons were similar. More heterogeneity between sexes was observed in the distal colon where potentiation of neuron responses in descending circuits was prominent in males and potentiation of those associated with ascending and circumferential circuits was more evident in females. However, other effects were consistent between sexes such as cFTS, which recruited more neurons

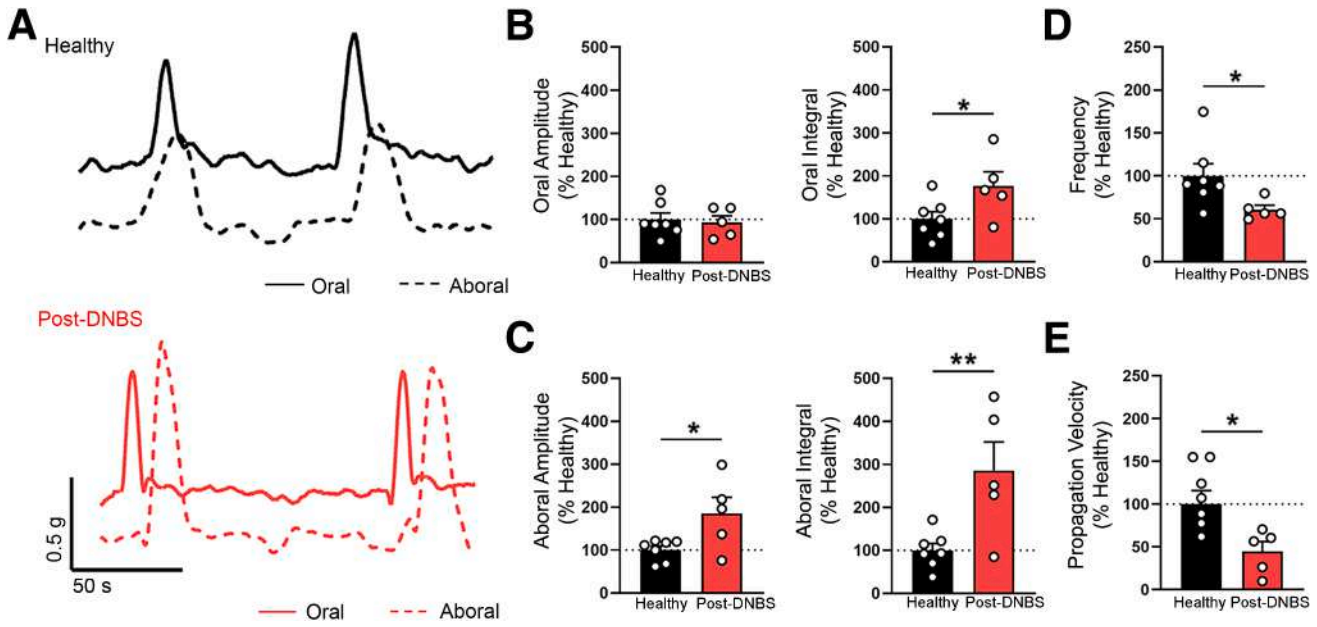


**Figure 2. Experiencing acute inflammation promotes persistent gut dysfunction.** (*A*) Representative CMC recordings in colons from healthy mice and those that experienced DNBS colitis. Solid and dashed lines represent oral and aboral recording sites, respectively. Summary of CMC characteristics including oral contraction amplitude and integral, respectively (*B*), and aboral contraction amplitude and integral (*C*), respectively. CMC frequency (*D*), and propagation velocity (*E*). Unpaired *t*-test; $^{*}P < .05$, $^{**}P < .01$; n = 5–7 animals/group. Data are presented as mean ± SEM.

in the distal colon of both males and females following colitis.

Together, these data agree with prior electrophysiological studies and extend them to show that experiencing an acute bout of inflammation creates persistent region- and circuit-specific hyperexcitability in functional enteric motor neurocircuits. This effect involves facilitation of neuron-to-neuron communication and increased excitability of neuron subsets.

## *Enteric Glia Are More Responsive to Neuron Activity Following Colitis*

Enteric glia surround enteric neurons in gut motor neurocircuits and bidirectional communication between enteric glia and neurons modulates gut motility.[20,41] Enteric glia detect neuron activity on a synapse-by-synapse basis, and subsets of glia are functionally linked to polarized myenteric circuits,[34] which our data show are more excitable following inflammation. This suggests that neuron-to-glia communication could also be facilitated and contribute to network hyperexcitability, but this concept remains untested. Toward this end, we used $Ca^{2+}$ imaging to study glial activity evoked by stimulating polarized neural pathways in samples of myenteric plexus from healthy animals and those that experienced a prior bout of acute colitis as described above.

Experiencing intestinal inflammation caused a global increase in glial responsiveness to neuron activity throughout the entire colon (Figure 5*A, B, F–H* and Figure 6). This effect was most prominent in the distal colon but occurred throughout the entire colon. Glial responses to descending neural pathway stimulation increased by 147% in the distal colon and by 64% in the proximal colon after inflammation (Figure 6*A–D*). Likewise, glial responses to ascending neural pathways increased by 86% in the distal colon and 66% in the proximal colon (Figure 6*F–I*). The most marked differences were observed in glial responses evoked by neurons in circumferential pathways. Here, glial $Ca^{2+}$ responses surged by 393% in the distal colon and by 102% in the proximal colon (Figure 5*B, F, and G*). Augmented glial responses to neuron activity following inflammation in the distal colon were also associated with greater glial recruitment in response to descending (Figure 6*E*), ascending (Figure 6*J*), and circumferential (Figure 5*H*) pathway stimulation.

Segregating the data by sex and colonic region revealed some nuances in changes to glial responsiveness between pathways and colonic regions in males and females (Table 2). Glial responses to neuron activity in descending pathways were increased throughout the colon in both sexes following inflammation, and more glia were stimulated in response to descending pathway activation in the distal post-inflamed colon. Glia exhibited larger amplitude $Ca^{2+}$ responses to ascending and circumferential pathway stimulation in the post-inflamed proximal colon in both sexes and the number of responding glia increased in females. The amplitude of glial $Ca^{2+}$ responses was greater when ascending and circumferential pathways were stimulated in the distal post-inflamed colon, but more glia responded to ascending pathway stimulation in males and more to circumferential circuits in females.

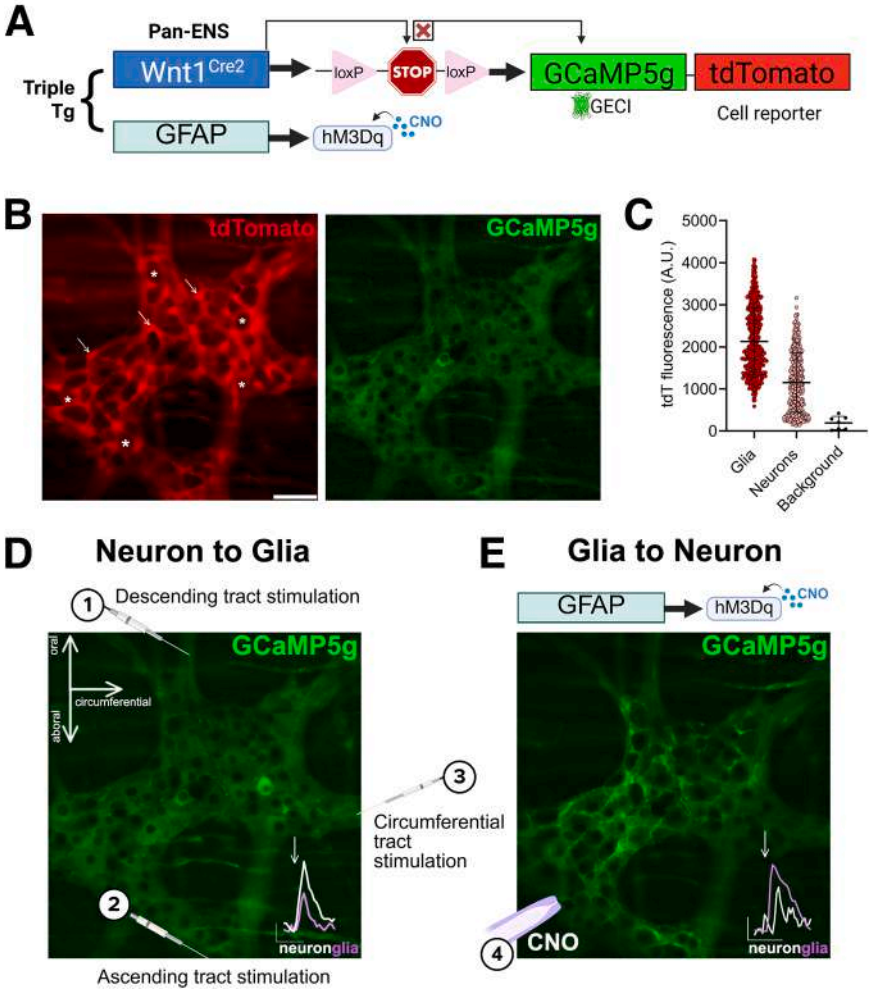


**Figure 3. *Wnt1*$^{Cre2;GCaMP5g\text{-}tdT}$*;GFAP::hM3Dq* mice and experimental approaches to study neuron-glia communication.** (*A*) Genetic construct of the triple transgenic mouse line in which expression of GCaMP5g and tdTomato is driven in Wnt1+ cells (pan-enteric neuron and glia) and expression of the chemogenetic receptor hM3Dq is driven in GFAP+ enteric glia. (*B*) Representative images showing tdTomato and GCaMP5g expression in a myenteric ganglion. Examples of neurons and glia are highlighted by *asterisks* and *arrows*, respectively. (*C*) Quantification of tdTomato expression in neurons (n = 385) and glia (n = 430) showing that tdTomato expression is more robust in enteric glia but still detectable in enteric neurons. N = 7 ganglia, from 2 mice. (*D–E*) Illustration of experimental approaches whereby ascending, descending, and circumferential neural pathways were stimulated by FTS (*D*) or glia were activated by CNO (*E*). FTS stimulates neuron-to-glia signaling (*D*, *bottom traces*) whereas CNO drives glia-to-neuron communication (*E*, *bottom traces*). Scale bar = 25 $\mu$m.

Together, these observations show that glia are more responsive to neuron activity following colitis. This effect is most prominent in enteric motor neurocircuits of the distal colon close to the initial site of injury and when neurons associated with circumferentially oriented pathways are stimulated. Therefore, persistent facilitation of neuron-to glia communication is an ongoing feature of the ENS following inflammation.

## *Hyperactive Enteric Glia Drive Abnormal Excitatory Neuronal Responses and Motor Dysfunction Following Colitis*

The results to this point show that inflammation produces persistent hyperactivity in enteric motor neurocircuits that involves facilitation of neuron-to-glia communication. Increased glial responsiveness to neuron activity could result from noncell autonomous changes to neurons that increase excitatory neurotransmitter drive to glia and/or cell autonomous changes to glia that increase glial responsiveness to transmitters. To differentiate between these possibilities and understand whether glia exhibit cell autonomous changes in excitability following inflammation, we used chemogenetics to selectively stimulate glial Gq signaling by focal CNO application in samples from *Wnt1*$^{Cre2;GCaMP5g\text{-}tdT}$*;GFAP-hM3Dq* mice (Figure 7*A*). As shown in our prior work,[34] direct glial stimulation produced robust glial $Ca^{2+}$ responses among myenteric glia in the proximal and distal colon (Figure 7*B*). Glial responses to CNO were amplified in samples from post-inflamed mice in which glial response amplitudes were 78% larger in the proximal colon and 87% larger in the distal colon (Figure 7*B–D*). Experiencing inflammation also increased the fraction of glia responding to CNO in the distal colon by 28% (Figure 7*E*). These data show that enteric glia exhibit cell autonomous changes following inflammation that increases their excitability. Therefore, ENS hyperexcitability following inflammation involves changes to both neurons and glia that facilitate intercellular communication.

Once stimulated, enteric glia exert reciprocal effects on neurons that affect the strength of neurotransmission in myenteric neurocircuits.[20,34,42] Given that enteric glia are hyperexcitable following inflammation, we reasoned that they may also exert abnormal excitatory influences over enteric neurons. In agreement with prior work,[34] stimulating glia in samples from animals that experienced inflammation produced exaggerated effects on enteric neurons and elicited neuronal responses that were 37%

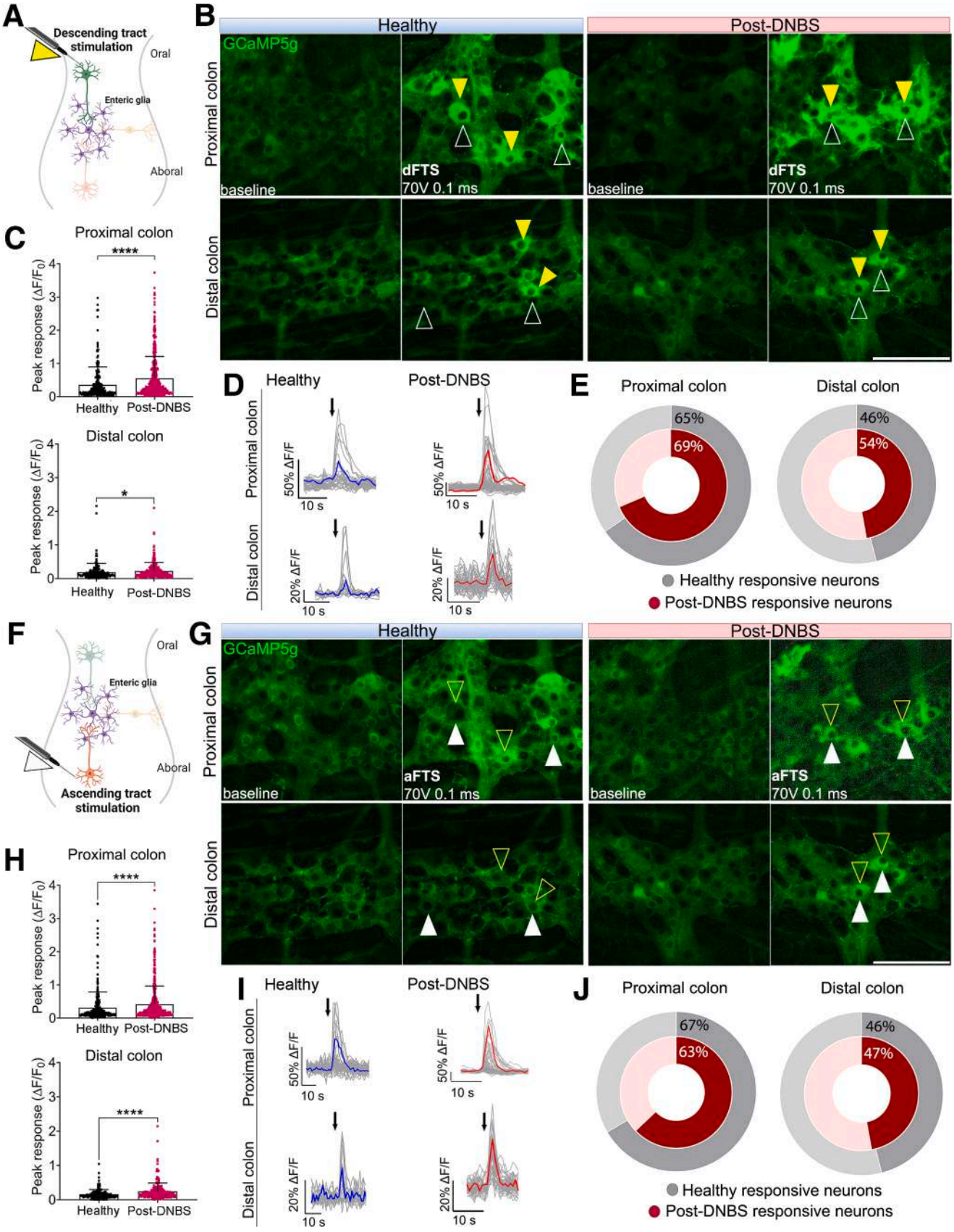
A
Descending tract stimulation
Oral
Enteric glia
Aboral
B
Healthy
Post-DNBS
GCaMP5g
Proximal colon
Distal colon
baseline
dFTS
70V 0.1 ms
C
Proximal colon
Peak response (ΔF/F0)
****
Healthy
Post-DNBS
Distal colon
*
D
Healthy
Post-DNBS
Proximal colon
Distal colon
50% ΔF/F
20% ΔF/F
10 s
E
Proximal colon
Distal colon
65%
69%
46%
54%
Healthy responsive neurons
Post-DNBS responsive neurons
F
Oral
Enteric glia
Aboral
Ascending tract stimulation
G
aFTS
H
I
J
67%
63%
47%

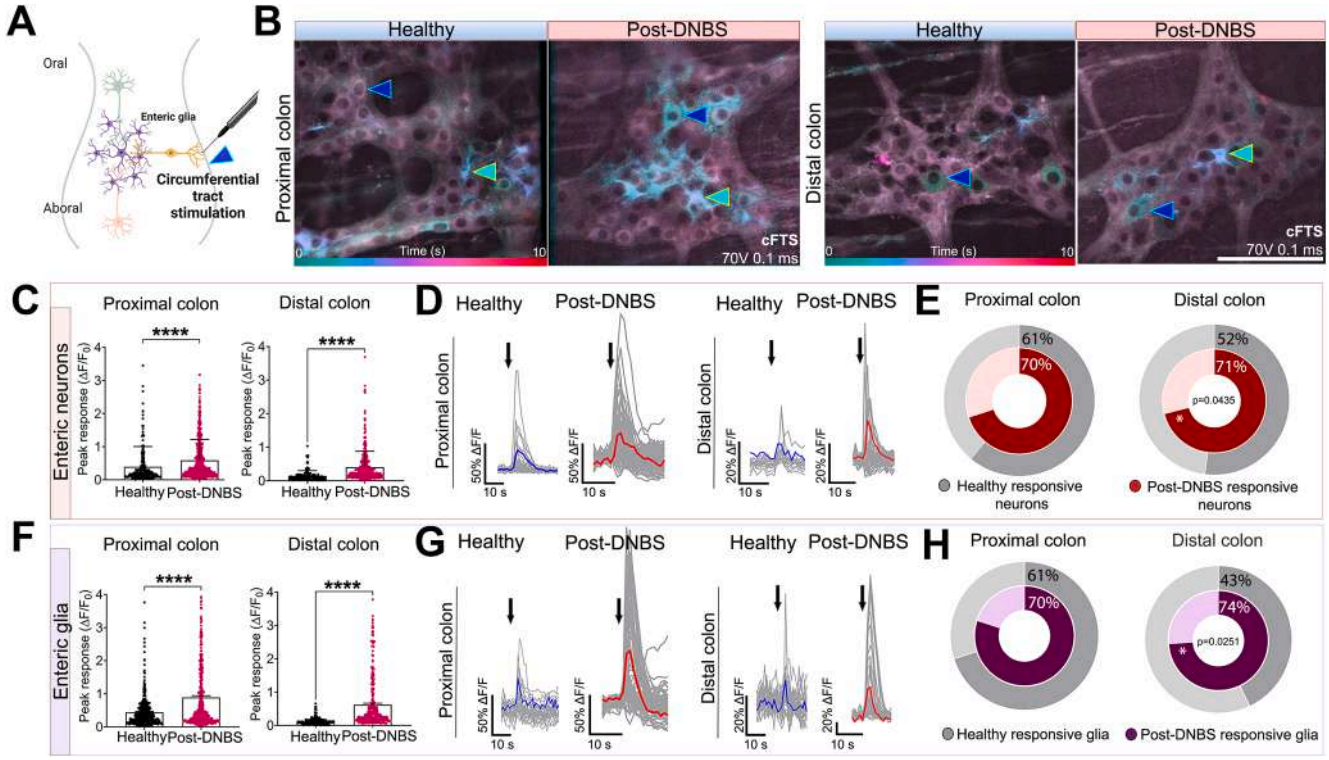


**Figure 5. Hyperexcitability of circumferentially oriented myenteric neural circuits after colitis.** (*A*) Illustration depicting cFTS in the myenteric plexus. (*B*) Representative images showing cellular activity (temporal color-coded activity over time) evoked by cFTS (70V, 0.1 ms cFTS) in myenteric ganglia of proximal and distal colon from healthy and post-DNBS *Wnt1*$^{Cre2;GCaMP5g\text{-}tdT}$*;GFAP-hM3Dq* mice. *Dark blue arrowheads* mark cFTS-activated neurons and *light blue* point cFTS-activated glia, respectively. Average peak $Ca^{2+}$ response evoked by cFTS in neurons (*C*) and glia. (*F*) Representative traces for neurons (*D*) and glia (*G*) show individual cells in *gray* and ganglionic average responses in *blue* for healthy and *red* for post-DNBS, respectively. *Black arrows* indicate the time of cFTS. Pie charts show the percentage of cFTS-responsive neurons (*E*) and glia (*H*). Only significant differences are indicated by *P* values in the pie charts. Mann-Whitney *U* test and unpaired *t*-test, ****$P <$ .0001; n = 250–500 proximal neurons, n = 150–300 distal neurons, n = 400–420 proximal glia, n = 220–350 distal glia from 5–6 animals/group. Data are presented as mean ± SD. Scale bar: 50 $\mu$m.

larger in amplitude in the proximal colon and 22% larger in amplitude in the distal colon (Figure 7*B, F, and G*). However, the overall percentage of neurons responding to glial stimulation remained comparable (Figure 7*H*). Therefore, hyperexcitable glia have the capacity to exert abnormal excitatory influences on enteric neurons that could contribute to neuronal hyperexcitability and network dysfunction following inflammation.

If hyperactive glia have an increased capacity to excite enteric neurons following inflammation, then stimulating glia should produce exaggerated motor responses under these conditions. In agreement, stimulating glia with CNO caused profound motor responses during $Ca^{2+}$ imaging experiments in samples of distal colon from mice that experienced colitis that were not observed in healthy controls (Figure 7*I and J*). Interestingly, although directly stimulating neural pathways with dFTS (Figure 8*A*), aFTS (Figure 8*B*), and cFTS (Figure 8*C*) also produced greater motor responses post-colitis, these effects were more heterogenous and were most evident when stimulating

**Figure 4.** (***See previous page***). **Hyperexcitability of descending and ascending neural circuits in the myenteric plexus following colitis.** (*A*) Illustration depicting dFTS in the myenteric plexus. (*B*) Representative images of basal and peak evoked cellular activity (70V, 0.1 ms dFTS) as reported by the genetically encoded $Ca^{2+}$ indicator GCaMP5g in myenteric ganglia from healthy and post-DNBS *Wnt1*$^{Cre2;GCaMP5g\text{-}tdT}$*;GFAP-hM3Dq* mice. *Solid yellow arrows* highlight neurons activated by dFTS. *Clear white arrows* show neurons that respond to aFTS in *G*. Summary data showing neuron response amplitudes (*C*), representative traces of neuronal activity in one ganglion (*D*), and percentages of responding neurons (*E*) in proximal and distal colon from healthy and post-colitis mice. Individual neuronal responses are shown in *gray traces* in *D*, whereas averages are shown in *blue* for healthy and *red* for post-DNBS. *Black arrows* indicate the time of dFTS. (*F*) Illustration depicting aFTS. (*G*) Representative images showing activity evoked by aFTS (70V, 0.1 ms aFTS) in the same ganglia shown in *B*. *Solid white arrows* highlight neurons activated by aFTS. *Clear yellow arrows* indicate neurons that responded to dFTS as shown in *B*. Neuron response amplitude (*H*), representative traces of ganglionic neuronal activity (*I*), and pie charts showing percentages of neurons responding to aFTS (*J*). Only significant differences are indicated by *P* values in the pie charts. Mann-Whitney *U* test and unpaired *t*-test, *$P <$ .05 and ****$P <$ .0001; n = 250–500 proximal cells, n = 100–200 distal cells from 5–6 animals. Data are presented as mean ± SD. Scale bar: 50 $\mu$m.

**Table 1.** Comparison of Neuronal $Ca^{2+}$ Responses in Healthy vs Post-DNBS Mice Stratified by Region and Sex

| | | Neurons | | | | | | | |
|---|---|---|---|---|---|---|---|---|---|
| | | Proximal colon | | | | Distal colon | | | |
| Stimuli | | Healthy male | DNBS male | Healthy female | DNBS female | Healthy male | DNBS male | Healthy female | DNBS female |
| dFTS | Amplitude (ΔF/F) | 0.40 ± 0.59 | 0.72 ± 0.80[c] | 0.18 ± 0.21 | 0.43 ± 0.51[c] | 0.19 ± 0.31 | 0.26 ± 0.24[b] | 0.18 ± 0.14 | 0.21 ± 0.25 |
| | % cells | 67 ± 18.7 | 85 ± 11 | 63 ± 22 | 62 ± 16.9 | 64 ± 27.3 | 65 ± 10.8 | 37 ± 5.3 | 41 ± 20.4 |
| aFTS | Amplitude (ΔF/F) | 0.36 ± 0.55 | 0.62 ± 0.72[c] | 0.19 ± 0.15 | 0.30 ± 0.36[a] | 0.13 ± 014 | 017 ± 0.17 | 0.18 ± 0.13 | 0.26 ± 0.26[b] |
| | % cells | 68 ± 26.9 | 66.60 ± 15.6 | 65 ± 10 | 61 ± 13.3 | 61 ± 16.3 | 49 ± 16.1 | 35 ± 10.8 | 49 ± 19.1 |
| cFTS | Amplitude (ΔF/F) | 0.44 ± 0.68 | 0.87 ± 0.78[c] | 0.24 ± 0.29 | 0.43 ± 0.45[c] | 0.10 ± 0.13 | 0.37 ± 0.49 | 0.19 ± 0.17 | 0.41 ± 0.47[c] |
| | % cells | 63 ± 16.9 | 75 ± 22.3 | 56 ± 8.4 | 67 ± 13.4 | 68 ± 28.5 | 73 ± 26.4[c] | 39 ± 17.2 | 70 ± 18.7[a] |
| CNO | Amplitude (ΔF/F) | 0.46 ± 0.34 | 0.72 ± 0.49[c] | 0.46 ± 0.22 | 0.56 ± 0.39 | 0.32 ± 0.36 | 0.45 ± 0.22[c] | 0.53 ± 0.42 | 0.55 ± 0.41 |
| | % cells | 76 ± 33.8 | 93 ± 6.3 | 91 ± 12.3 | 92 ± 8.7 | 83 ± 20.4 | 93 ± 10.3 | 76 ± 20 | 96 ± 6 |

aFTS, ascending focal tract stimulation; cFTS, circumferential focal tract stimulation; CNO, clozapine-N-oxide; dFTS, descenting focal tract stimulation; DNBS, 2,4-di-nitrobenzene sulfonic acid.
[a].05
[b].01
[c].0001

circumferential neural pathways with cFTS, whereas those stimulated by aFTS showed no change. These effects suggest that glial hyperexcitability may exert broad excitatory influences over multiple neuron subtypes in myenteric neurocircuits to produce motor responses that are equal to, or greater than directly stimulating hyperactive IPANs.

To understand if these effects translate to organ-level changes in motor function, we assessed the effects of stimulating glia with CNO on CMC activity in colons from healthy and post-inflamed mice (Figure 9). In line with our prior studies,[42,43] stimulating glia enhanced the size of CMC contractions (Figure 9*A, D, F, G*) and increased CMC frequency (Figure 9*E*) in healthy organs. Multiple parameters of CMCs were increased in post-inflamed colons (Figure 2), suggesting ongoing hyperexcitability of the neural circuits that control CMC activity. Under these conditions, stimulating glia further exacerbated excitatory aspects of CMC activity in the distal colon, but not in the proximal colon (Figure 9*B, F, G*). Interestingly, inflammation reduced CMC frequency and glial stimulation was not sufficient to overcome this effect (Figure 9*E*). Together, these data show that hyperexcitable glia gain abnormal excitatory influences over enteric motility neurocircuits that contribute to, and amplify, dysmotility following inflammation.

## *Glial Hyperexcitability Involves Reduced Nitrergic Suppression, $PGE_2$ Signaling, and Enhanced Glial Connexin-43 Activity*

Our data show that persistent glial hyperexcitability following colitis contributes to abnormal motor behavior by enhancing the excitatory influence of gliotransmission on enteric neurons. Enhanced excitatory aspects of gut neuromuscular transmission following colitis are thought to be mediated, in part, by a loss of tonic inhibition by nitrergic neurons.[17,19] Therefore, we tested whether impaired nitrergic signaling contributes to glial hyperexcitability following colitis. In support, abnormally large glial $Ca^{2+}$ responses to CNO in post-inflamed samples were suppressed by the NO donor propylamine propylamine NONOate (PAPA NONOate) in the proximal colon (Figure 10*A, B, and D*) and by the cell-permeable cyclic guanosine 3′:5′-monophosphate (cGMP) analog 8-Br-cGMP in the distal colon (Figure 10*A, B, and E*). Neuronal responses subsequent to glial stimulation by CNO were also dampened, without changes to the overall numbers of glia and neurons stimulated (Figure 10*A, C, F, and G*). PAPA NONOate had no effect on glial or neuronal responses to CNO in samples from healthy animals, but 8-Br-cGMP did exhibit suppressive effects in the healthy proximal colon that could indicate NO-independent signaling roles of cGMP or greater drug efficacy in this region. These results suggest that restoring nitrergic tone after inflammation can partially constrain glial hyperactivity; however, additional mechanisms beyond the loss of nitrergic inhibition likely contribute to post-inflammatory glial hyperexcitability.

Enteric glia influence neuron activity through mechanisms that include gliotransmitter release through membrane channels composed of connexin-43 (Cx43).[44] Given that enhanced glial Cx43-mediated signaling contributes to enteric neuron death and sensory neuron hypersensitivity during acute colitis,[23,26] we speculated that persistent changes to glial Cx43 activity contribute to augmented

effects of glia on gut neuromuscular transmission following colitis. Assessing glial Cx43 hemichannel permeability using the established ethidium bromide (EtBr) dye uptake assay[23,44–46] showed that glial Cx43 hemichannel opening was increased by 43% following inflammation (Figure 11*A and B*, images *a'* and *a''*). Blocking Cx43 hemichannels with

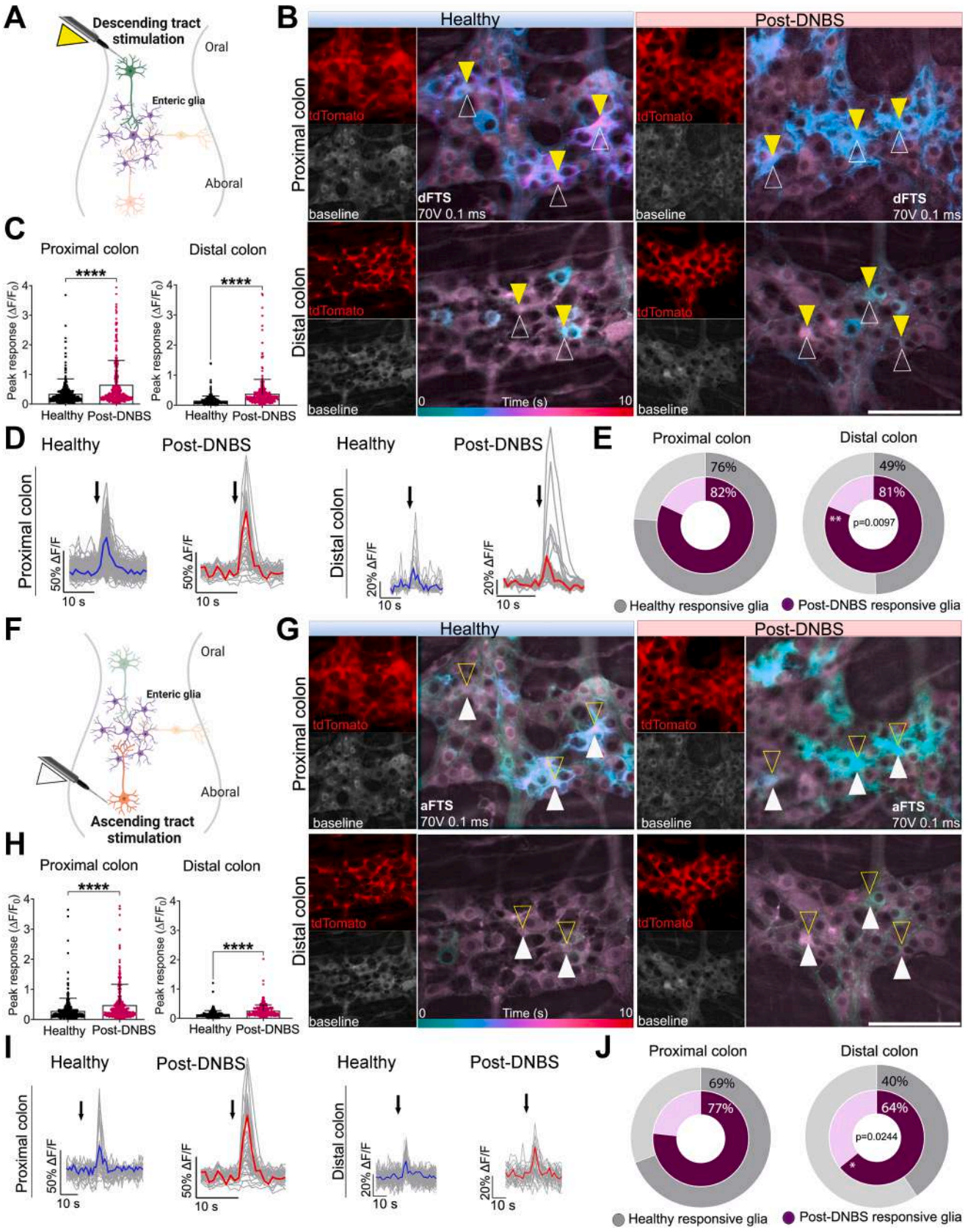

**Table 2.** Comparison of Glial $Ca^{2+}$ Responses in Healthy vs post-DNBS Mice Stratified by Region and Sex

| | | Glia | | | | | | | |
|---|---|---|---|---|---|---|---|---|---|
| | | Proximal colon | | | | Distal colon | | | |
| Stimuli | | Healthy male | DNBS male | Healthy female | DNBS female | Healthy male | DNBS male | Healthy female | DNBS female |
| dFTS | Amplitude (ΔF/F) | 0.40 ± 0.58 | 1.15 ± 1.18[d] | 0.21 ± 0.17 | 0.51 ± 0.63[d] | 0.17 ± 0.20 | 0.30 ± 0.28[d] | 0.13 ± 0.08 | 0.40 ± 0.53[d] |
| | % cells | 80 ± 14.1 | 82 ± 9.3 | 70 ± 23.5 | 82 ± 15.2 | 68.12 ± 22.5 | 84 ± 3.5 | 42 ± 15.12 | 80 ± 16.7[b] |
| aFTS | Amplitude (ΔF/F) | 0.32 ± 0.52 | 0.77 ± 1.02[d] | 0.23 ± 0.17 | 0.31 ± 0.30[b] | 0.14 ± 0.15 | 0.15 ± 0.08[a] | 0.13 ± 0.09 | 0.29 ± 0.21[d] |
| | % cells | 78 ± 17.5 | 79 ± 2.2 | 58 ± 13.9 | 75 ± 9.5[a] | 50 ± 5.9 | 67 ± 4.1[b] | 40 ± 15.4 | 63 ± 24.3 |
| cFTS | Amplitude (ΔF/F) | 0.47 ± 0.55 | 1.52 ± 1.45[d] | 0.32 ± 0.47 | 0.58 ± 0.63[d] | 0.08 ± 0.08 | 0.58 ± 0.67[d] | 0.15 ± 0.10 | 0.63 ± 0.79[d] |
| | % cells | 81 ± 18.4 | 81 ± 8.9 | 53 ± 23.5 | 79 ± 9.8[a] | 52 ± 25.3 | 53 ± 40.5 | 36 ± 18 | 84 ± 9.3[c] |
| CNO | Amplitude (ΔF/F) | 0.50 ± 0.54 | 1.40 ± 0.71[d] | 0.96 ± 0.36 | 0.97 ± 0.58 | 0.80 ± 0.56 | 1.07 ± 0.50[d] | 0.33 ± 0.37 | 1.09 ± 0.38[d] |
| | % cells | 85 ± 17.3 | 97 ± 4.5 | 90 ± 5.2 | 94 ± 4.4 | 59 ± 18.3 | 96 ± 8.2 | 82 ± 22.9 | 100 ± 0[b] |

aFTS, ascending focal tract stimulation; cFTS, circumferential focal tract stimulation; CNO, clozapine-N-oxide; dFTS, descenting focal tract stimulation; DNBS, 2,4-di-nitrobenzene sulfonic acid.
[a].05
[b].01
[c].001
[d].0001

the mimetic peptide 43Gap26 reduced glial dye uptake but did not completely abolish glial permeability (Figure 11*A and B, image a'''*). This could suggest either reduced efficacy of 43Gap26 due to changes in channel configuration or activation of additional membrane channels. Glial activation by CNO normally increases Cx43-mediated permeability in healthy animals[23] but had no additional impact on dye uptake in samples from post-inflamed mice treated with DNBS (Figure 11*A and B, images a'''' and a''''*). This could indicate a ceiling effect whereby hemichannel function is already maximized following inflammation. Persistent facilitation of gliotransmitter release mechanisms such as Cx43 shown here in combination with glial hyperexcitability give glia a greater potential to influence responses in the surrounding enteric neurons.

Cx43 regulates glial intercellular communication by controlling the release of gliotransmitters such as $PGE_2$.[23,47] During inflammation, glial $PGE_2$ release is enhanced by proinflammatory cytokines, and $PGE_2$ signaling drives persistent hyperexcitability of myenteric IPANs.[12] Thus, we tested whether $PGE_2$ contributes to IPAN and glial hyperreactivity post-inflammation by using cFTS to activate IPANs while selectively blocking EP3 and EP4 $PGE_2$ receptors with the antagonists L-798, 106 and L-161, 982. Glial $Ca^{2+}$ responses to circumferential pathway activation were markedly decreased in the post-inflamed mice in the presence of EP3 and EP4 antagonists, but not in the healthy controls (Figure 11*C–E*). Likewise, EP3 and EP4 antagonists decreased neuronal $Ca^{2+}$ responses driven by circumferential pathway activation (Figure 11*F and G*) and glial stimulation via CNO (Figure 11*H and I*) in the post-inflamed colon. Together, these findings support the conclusion that $PGE_2$ contributes to glial hyperexcitability and interactions with circuits dominated by IPANs.

**Figure 6.** (***See previous page***). **Enteric glia are more responsive to descending and ascending neural circuits after colitis.** (*A*) Schematic of dFTS in the myenteric plexus. (*B*) Representative images showing glial activity at rest (baseline) and after dFTS (70V, 0.1 ms dFTS) in proximal and distal colon from healthy and post-DNBS *Wnt1*$^{Cre2;GCaMP5g\text{-}tdT}$*;GFAP-hM3Dq* mice. Glia were identified based on morphology and tdTomato expression. $Ca^{2+}$ responses are shown as temporally color-coded activity over time images. *Solid yellow arrows* indicate active glia. *Clear white arrows* show glia that respond to aFTS in *G*. Glial response amplitude (*C*), representative traces of activity (*D*), and summary plots of percentages of dFTS-responsive glia in the proximal and distal colon (*E*). *Gray traces* show individual cells with averaged responses overlaid in *blue* for healthy and *red* for post-DNBS. *Black arrows* indicate the time of dFTS. (*F*) Illustration of aFTS. (*G*) Representative images showing activity evoked by aFTS in the same ganglia as shown in *B*. *Solid white arrows* show glia stimulated by aFTS. *Clear white arrows* show glia that respond to dFTS in *B*. Glial response amplitude (*H*), representative traces showing cellular responses (*I*), and summary plots showing percentages of glia responding to aFTS (*J*). Only significant differences are indicated by *P* values in the pie charts. Mann-Whitney *U* test and unpaired *t*-test, ****$P < .0001$; n = 360–400 proximal glia dFTS, n = 250–260 distal glia dFTS; n = 400–478 proximal glia aFTS, n = 300–315 distal glia aFTS from 5–6 animals/group. Data are presented as mean ± SD. Scale bar = 50 $\mu$m.

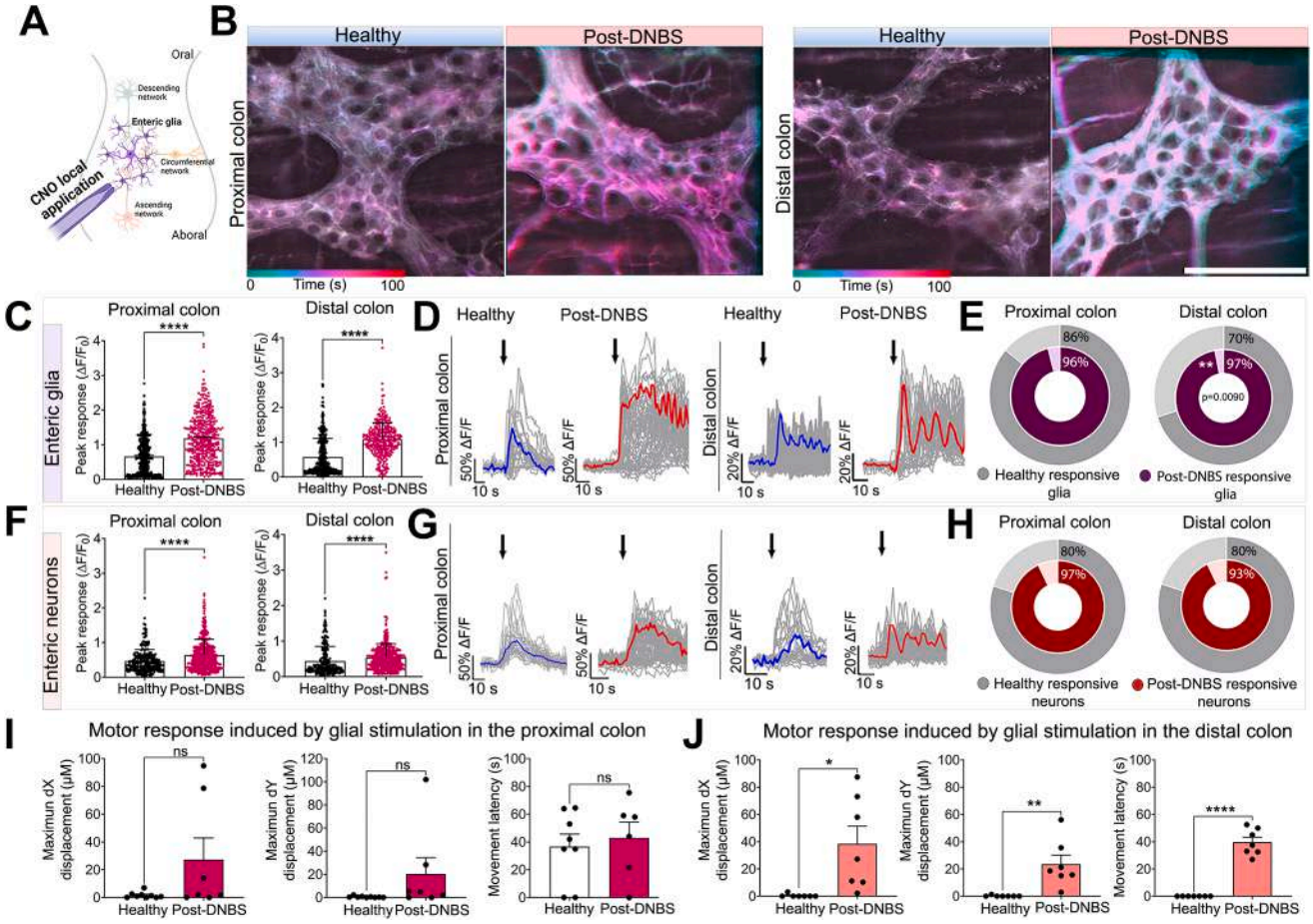


**Figure 7. Enteric glia exhibit intrinsic hyperexcitability after colitis.** (*A*) Schematic showing selective glial stimulation via focal CNO application to ganglia in *Wnt1*$^{Cre2;GCaMP5g\text{-}tdT}$*;GFAP-hM3Dq* mice. (*B*) Representative images showing temporally color-coded $Ca^{2+}$ responses evoked by CNO in proximal and distal ganglia from healthy and post-DNBS mice. Glial response amplitude (*C*), representative traces (*D*), and summary plots showing percentages of active glia in response to CNO (*E*). *Gray traces* show responses of individual cells with averaged responses overlaid in *blue* for healthy and *red* post-DNBS. *Black arrows* indicate the time of CNO application. (*F–H*) Neuron responses evoked by glial stimulation. Neuron response amplitude (*F*), representative traces showing neuron responses (*G*), and summary data showing percentages of neurons activated by stimulating glia with CNO (*H*). Only significant differences are indicated by *P* values in the pie charts. Mann-Whitney *U* test and unpaired *t*-test, $^{*}P < .05$, $^{**}P < .01$, $^{****}P < .0001$; n = 380–400 proximal glia, n = 315–370 distal glia; n = 360–400 proximal neurons, n = 250–260 distal neurons from 5–6 animals/group. (*I–J*) Motor responses (displacement [$\mu$m] and movement latency [s] to peak displacement) induced by glial stimulation with CNO in proximal and distal colon wholemounts. Unpaired *t*-test, n = 6–8 ganglia/group from 5–6 animals/group. Data are presented as mean ± SEM or SD. Scale bar: 50 $\mu$m.

## Discussion

Experiencing acute gastroenteritis is a potent driver of long-term gut dysfunction that contributes to the pathophysiology of IBS and IBD in remission. Prior work showed that inflammation changes gut functions through mechanisms that produce persistent neuroplasticity in enteric motor neurocircuits. Here, we build upon these findings to show that synaptically connected networks of enteric neurons are more excitable following colitis and stimulate greater activity among the surrounding enteric glia. Enteric glia exhibit cell autonomous changes to become intrinsically hyperexcitable following inflammation and have a greater potential to exert excitatory effects on the surrounding neurons. This abnormal excitatory drive from glia contributes to ongoing network hyperexcitability and abnormal gut motility following inflammation. Changes in glial excitability involve reduced nitrergic inhibition, potentiation of gliotransmission release mechanisms, and $PGE_2$ signaling. These effects unleash a gain in the excitatory nature of gliotransmission that enhances subsequent excitatory effects on enteric neurons and motor responses. Together, these observations point to glia as an important contributor to persistent gut dysmotility following inflammation.

Experiencing a bout of acute gastroenteritis causes persistent changes in gut motility, secretions, and sensations by promoting neuroplasticity among intrinsic and extrinsic neurons that innervate the gut.[27] Changes to

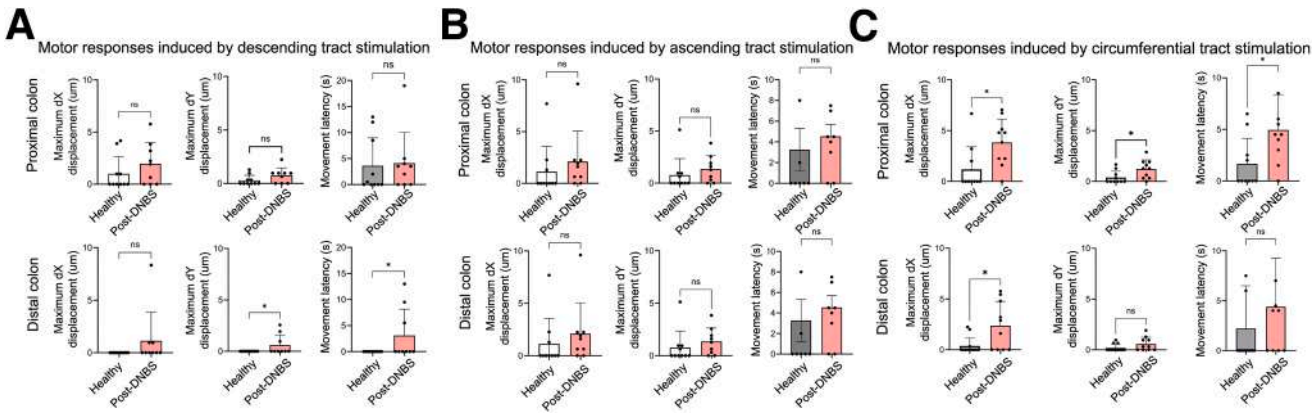


**Figure 8. Motor responses evoked by descending, ascending and circumferential focal tract stimulation in circular muscle-myenteric plexus whole-mount preparations during $Ca^{2+}$ imaging experiments.** The first and second lines in each panel show quantification of tissue movement in proximal and distal colon, respectively. Displacement was measured in pixels and converted to $\mu$m to describe tissue movement. Motor effects were evoked by (*A*) descending, (*B*) ascending, and (*C*) circumferential focal tract stimulation during $Ca^{2+}$ imaging experiments. Unpaired *t*-test, $^{*}P < .05$. n = 8–10 ganglia from 3–4 mice. Data are presented as mean ± SEM.

enteric neurons include hyperexcitability among submucosal and myenteric IPANs,[11,12] facilitated synaptic transmission,[16,33] a loss of viscerofugal neurons,[48] and a loss of inhibitory motor neurons.[18,19] Mechanisms underlying these changes include actions of $PGE_2$ derived from COX-2,[12,49] a presynaptic increase in PKA activity,[33] an increase in ionic flow through $I_h$ channels in IPANs,[11,32] and inhibitory neuron death driven by glia in a process mediated by ATP, P2X7 receptors, and pannexin-1 channels.[19,26] Our observations are consistent with these findings and show that abnormal motor function persists following the resolution of inflammation. This effect involves facilitation of neuron-to-neuron communication and increased neuronal excitability in enteric motor neurocircuits. The most pronounced motor defects were observed in the distal colon, likely reflecting the closer proximity to the initial

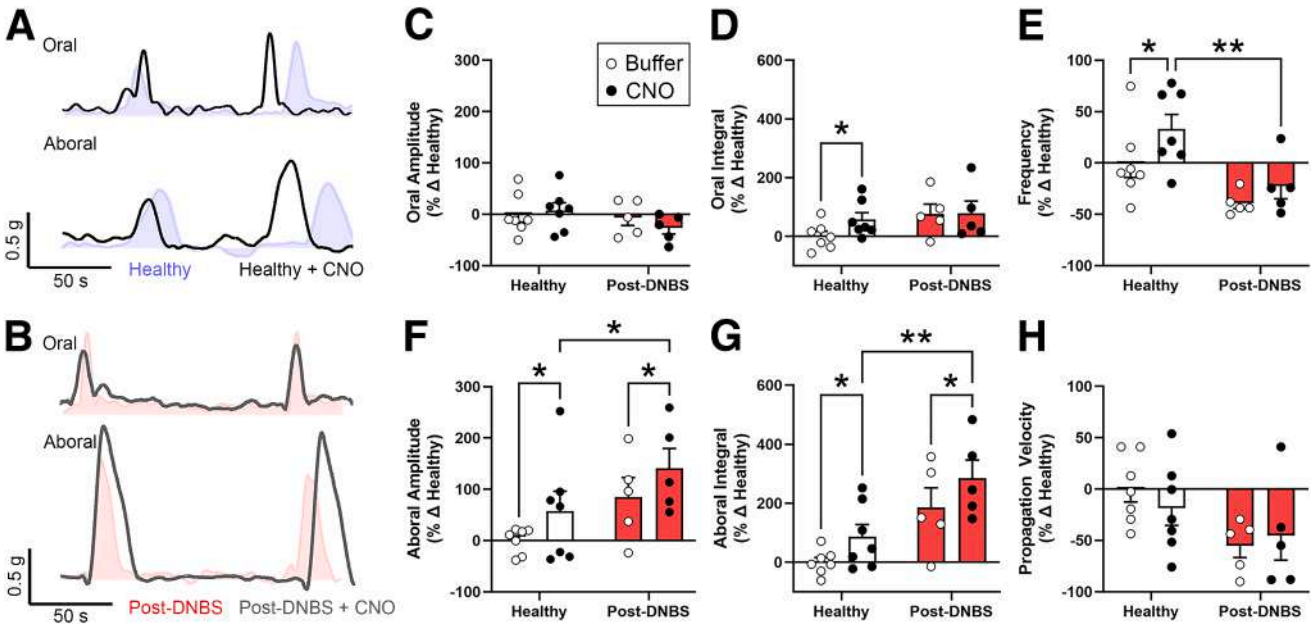


**Figure 9. Effects of stimulating enteric glia on CMC activity in healthy and post-DNBS colons.** Representative traces (*A, B*) and summary data (*C–H*) showing effects of glial stimulation via CNO on CMC activity in colons from healthy and post-inflamed *Wnt1*$^{Cre2;GCaMP5g\text{-}tdT}$*;GFAP-hM3Dq* mice. (*A*) Representative traces of CMC activity in a healthy colon before (*blue*) and after glial stimulation by CNO (*black*). (*B*) Representative traces of CMC activity from a post-DNBS colon before (*red*) and after glial stimulation (*gray*). Summary of CMC characteristics including oral contraction amplitude (*C*) and integral (*D*), CMC frequency (*E*), aboral contraction amplitude (*F*) and integral (*G*), and propagation velocity (*H*). Two-way ANOVA with Šídák's multiple comparisons test, $^{*}P < .05$, $^{**}P < .01$, n = 5–7 animals/group. Data are presented as mean ± SEM.

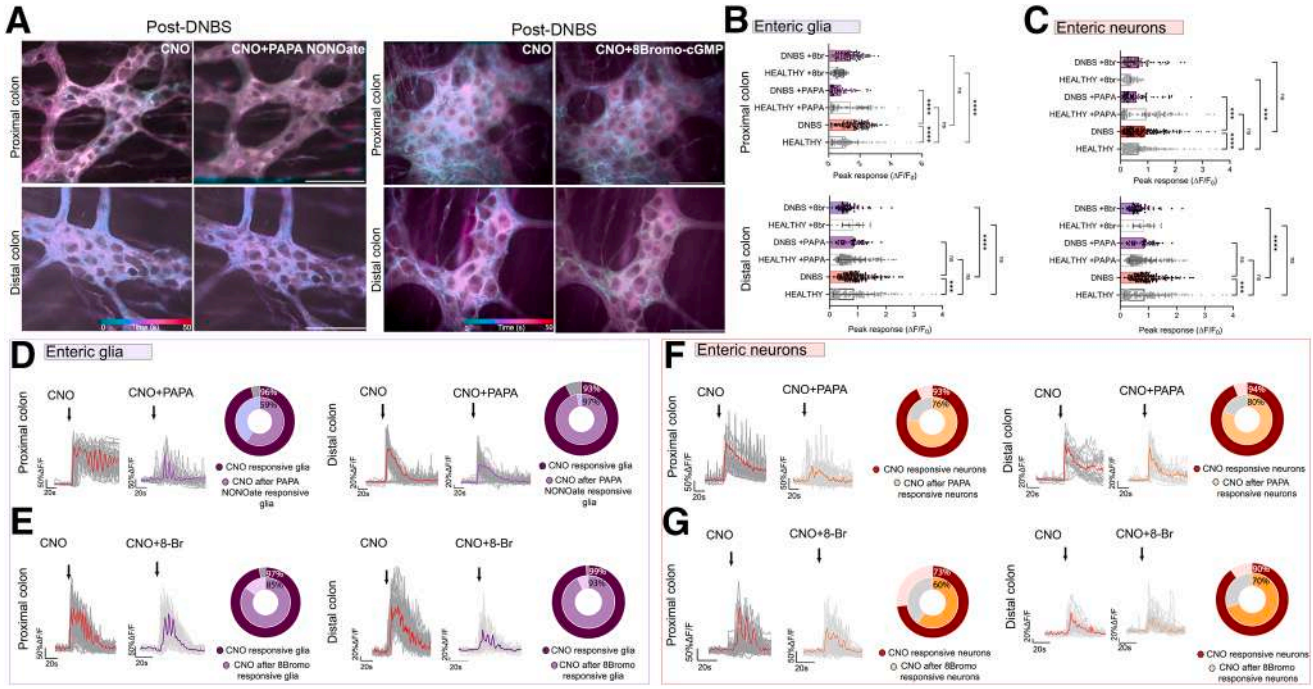


**Figure 10. Restoring nitrergic tone partially suppresses glial hyperexcitability and subsequent effects on neurons postinflammation.** (*A*) Representative temporally color-coded images showing effects of PAPA NONOate and 8Bromo-cGMP on $Ca^{2+}$ responses evoked by glial stimulation with CNO in the post-inflamed colon myenteric plexus. (*B*) Glial and (*C*) neuronal response amplitudes in healthy and post-inflamed samples. Kruskal–Wallis test followed by Dunn's multiple comparisons test, ***$P < .001$, ****$P < .0001$; n = 200–400 cells from 2–4 animals/group. (*D–G*) Representative traces and summary plots showing effects of PAPA NONOate and 8Bromo-cGMP on glial responses to CNO (*D, E*) and neuronal responses to glial stimulation by CNO (*F, G*) in post-inflamed samples. Only significant differences are indicated by *P* values in the pie charts. Unpaired *t*-test; n = 200–400 cells from 2–4 animals/group. Data are presented as mean ± SD. Scale bar: 50 $\mu$m.

inflammatory insult.[19] However, more distant sites in the proximal colon also exhibited clear hyperactivity among myenteric neurocircuits. This is particularly relevant for certain motor patterns of gut such as the CMC, which is thought to originate in pattern generator neural networks in the proximal colon.[31] Whether the long-range effects of localized inflammation involve broader activation of immune mechanisms or activation of synaptic pathways that promote neuroinflammation is unclear; however, prior work did show that intense activation of gut sensory neurons drives enteric neuroinflammation through actions on enteric glia.[21]

Crosstalk between enteric neurons and glia has emerged as a fundamental mechanism that regulates intestinal motor behaviors.[41] The extent of neuron-to-glia communication in the myenteric plexus is broad and involves transmitters released by neurons that engage glial receptors to drive activity in the form of intracellular $Ca^{2+}$ responses.[20,41] It is likely that most, if not all, glia within myenteric ganglia have the capacity to be stimulated by neurons; however, neuron-to-glia transmission, like neuron-to-neuron transmission, exhibits synaptic precision.[34] Specific subpopulations of myenteric glia are devoted to the synapses of polarized ascending and descending neural pathways in motor circuits, and to circumferential pathways dominated by multipolar IPANs.[34] Here, we show that glia exhibit enhanced responses to neurons in each of these pathways following inflammation. Augmented glial responses to polarized, unipolar ascending and descending circuits agrees with the concept of synaptic facilitation among S neurons in these pathways. However, glia showed the most marked increase in response to circumferential pathway activation. Stimulating circumferentially oriented fiber tracts preferentially activates enteric IPANs, which exhibit pronounced hyperactivity following inflammation.[11,15] IPANs are multipolar cells and have the potential to influence many glia within the myenteric plexus. Thus, a more prominent influence of IPAN pathways on glia following inflammation would be anticipated. Changes to glial responses involved an increase in glial response magnitudes and an increase in the proportion of glia recruited by neural circuits. Although the former might suggest an increased excitatory drive from neurons to glia, the latter suggests somewhat of a loss of specificity in neuron-to-glia transmission. Thus, mechanisms that should normally only enact glia whose subsequent effects would be confined to adjacent synapses would now gain influence over glia and synapses of surrounding pathways. This expanded recruitment of glia would contribute to an overall loss of precision in myenteric motor neurocircuits and disrupt motor functions. In agreement, we observed prominent disruptions to gut motor function in the distal colon where increased glial responsiveness to neuronal activity was most pronounced.

Increased glial responsiveness to neurons could result from either a gain in the excitatory drive from hyperactive neurons or an increase in the excitability of the glia themselves. Direct glial stimulation via chemogenetics circumvents the confounds of contributions by hyperactive neurons and revealed persistent hyperexcitability of

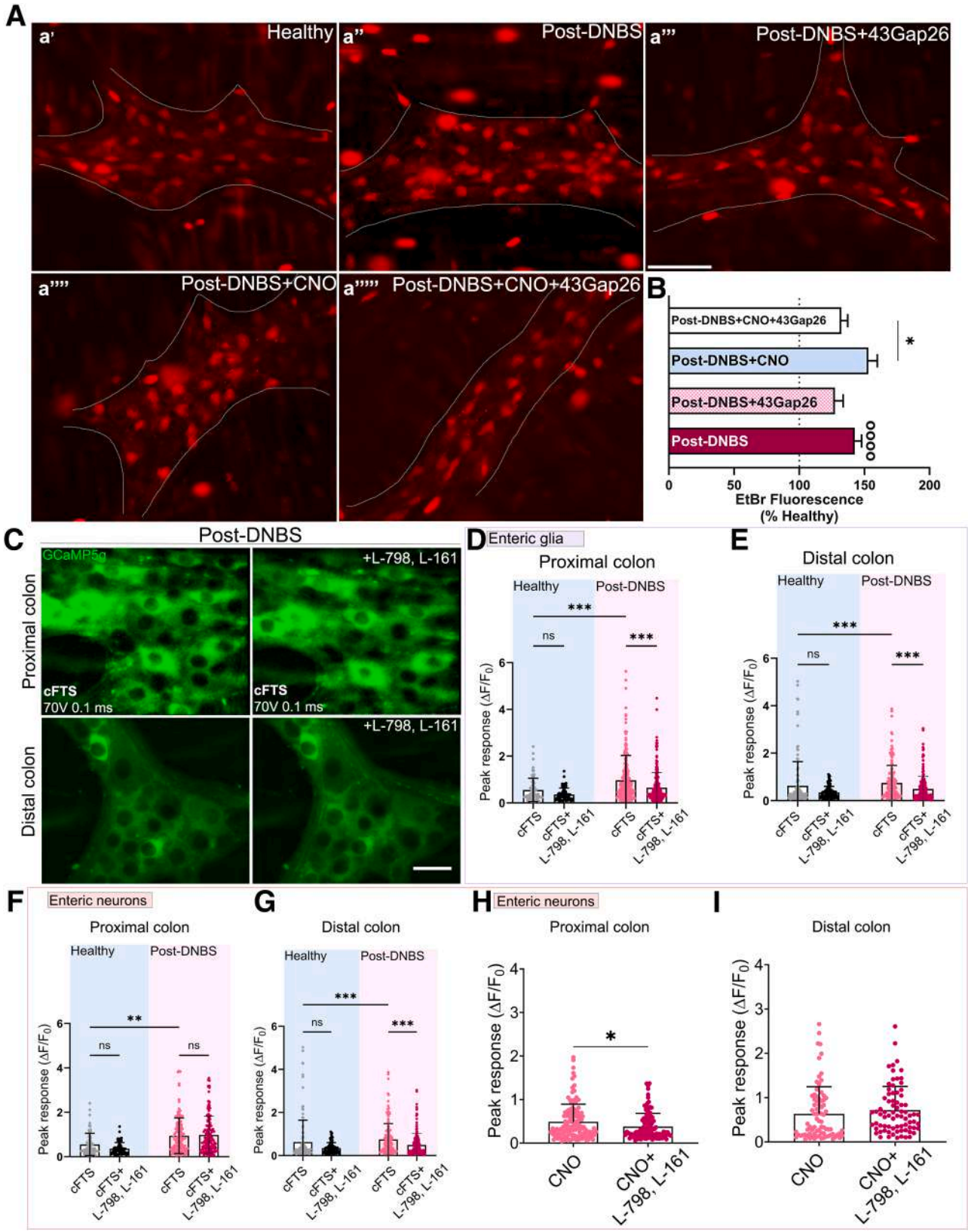

enteric glia following the resolution of inflammation. Thus, the effects of inflammation are imprinted in glia. How permanent this effect has remained unclear and will be an important area for future work. Enteric glia play an active role in the response to inflammation and changes undergone during reactive gliosis have the potential to alter enteric glial activities with either beneficial or detrimental effects on the surrounding neural and non-neuronal cells.[20] Similarly, astrocytes in the central nervous system (CNS) display profound changes in response to inflammation that amplifies astrocyte pro-inflammatory responses.[50,51] Pro-inflammatory cytokines induce metabolic remodeling in astrocytes that is integrated into epigenetic marks to control transcriptional responses.[52–54] Recent reports suggest that CNS-resident cells and cells recruited during inflammatory process may modulate astrocyte responses via the regulation of histone serotonylation.[55] These cell–cell interactions integrate multiple stimuli to regulate astrocyte epigenetic memory.[56–58] Whether similar mechanisms support the lasting effects of inflammation on enteric glial function is unknown; however, our findings support the possibility since greater glial responsiveness to direct stimulation via DREADDs were maintained following the resolution of inflammation and enteric glia within myenteric ganglia share functional similarities with astrocytes.

The main impact of hyperactive glia on gut motor function is an increased capacity to excite enteric neurons. Thus, stimulating glia under these conditions has the potential to produce exaggerated motor responses. Prior work supports the concept that enteric glia promote neuron hyperactivity through at least two distinct mechanisms. First, myenteric neuron hyperactivity is driven by mechanisms that involve $PGE_2$ and COX-2,[12,49] and our prior work showed that glia are the main source of these proinflammatory mediators in the myenteric plexus.[23] Second, glia drive inhibitory motor neuron death during inflammation[26] and inhibit the activity of remaining nitrergic neurons,[59,60] both of which release tonic inhibition of excitatory signaling in myenteric circuits. This raises the intriguing possibility that hyperactive glia are central in mechanisms that increase the overall excitability of motor circuits. In support, our data suggests that $PGE_2$ contributes to glial hyperexcitability through mechanisms that involve enhanced communication with IPANs. It has also been suggested that enteric glia are under tonic inhibition by nitrergic neurons,[61,62] and our data support this concept by showing that glial hyperexcitability involves a loss of tonic nitrergic suppression likely consequent to nitrergic neuron death following inflammation. Restoring nitrergic tone partially decreases glial activity and subsequent effects on surrounding neurons. Glial hyperexcitability also involves mechanisms that potentiate Cx43 hemichannels. Glial Cx43 hemichannel activity is potentiated by proinflammatory cytokines[23] and NO[26] during acute inflammation, and our current data show that glial Cx43 hemichannel permeability remains elevated despite the apparent resolution of inflammation. Enhanced glial hemichannel activity increases the ability of glia to secrete gliotransmitters such as ATP and $PGE_2$ that contribute to their enhanced excitatory influence on enteric neurons. This effect is similar to what has been observed in spinal cord astrocytes where increased Cx43 function and expression maintain late-phase neuropathic pain and neuron hyperexcitability.[63] The mechanisms that maintain Cx43 permeability in enteric glia remain unknown but likely involve glial proteins such as calcineurin that function to change the phosphorylation state of Cx43 and increase membrane permeability.[64,65] Regardless, this effect suggests that glia have a greater potential to release gliotransmitters, such as $PGE_2$, through mechanisms involving Cx43 hemichannels, which could contribute to neuronal hyperexcitability and motor dysfunction following inflammation.

There are certain limitations with the current work that warrant consideration. First, although we show that glial hyperactivity persists following the resolution of inflammation, it remains unclear how permanent inflammation-induced changes to glia are and whether they can be reversed. Second, it remains unclear whether the effects of acute intestinal inflammation primarily affect a specific subpopulation of enteric glia that is more sensitive to inflammatory insults or that has a specific role in regulating immune homeostasis. Identifying this specific glial subtype and exploring pharmacological strategies to modulate glial hyperexcitability could help develop more targeted therapeutic strategies for treating dysmotility in conditions such as IBS and IBD. Potential therapies that dampen glial hyperexcitability were already tested and include the PPAR$\alpha$ agonist palmitoylethanolamide,[66] cannabidiol,[67] pentamidine,[68] RAGE inhibitors,[69] and interleukin (IL)-1 receptor antagonists.[70,71]

In conclusion, our study identifies enteric glial hyperactivity as a mechanism of inflammation-induced

**Figure 11.** (***See previous page***). **Enteric glial hyperexcitability following colitis involves $PGE_2$ signaling and enhanced Cx43 activity.** (*A*) Representative images of Cx43-mediated EtBr dye uptake in enteric glia within myenteric ganglia from healthy (*a'*) and post-DNBS mice (*a''*). Effect of the Cx43 hemichannel inhibitor, 43Gap26 (10 $\mu$M), on dye uptake in post-DNBS myenteric plexus (*a'''*). Effect of glial stimulation via CNO on dye uptake in the myenteric plexus post-DNBS (*a''''*) and effect of 43Gap26 on dye uptake following glial stimulation (*a'''''*). Quantification of dye uptake normalized to healthy, unstimulated controls (*B*). Kruskal-Wallis followed by Dunn's multiple comparisons test, $^{\circ\circ\circ\circ}P < .0001$ for healthy vs post-DNBS; $^{*}P < .05$ for post-DNBS vs treatments; n = 8–16 ganglia from 8 animals/group. Data are presented as mean ± SEM. Scale bar: 100 $\mu$m. (*C*) Representative images of cFTS-evoked peak cellular activity (70V, 0.1 ms cFTS) in myenteric ganglia from post-DNBS *Wnt1*$^{Cre2;GCaMP5g\text{-}tdT}$*;GFAP-hM3Dq* mice. (*D–G*) Quantification of effects of EP3 and EP4 antagonists (L-798, 106, 10 $\mu$M; L-161, 982, 50 $\mu$M) on glial (*D–E*) and neuronal (*F–G*) responses to cFTS stimulation in samples from healthy and post-DNBS mice. Kruskal-Wallis followed by Dunn's multiple test, $^{***}P < .01$, $^{***}P < .001$, n = 180–220 cells from 3–4 mice for distal colon, and n ~ 100–300 cells from 3–4 mice for proximal colon analysis. (*H–I*) Effects of EP3 and EP4 antagonists on neuronal responses to glial stimulation driven by CNO in post-inflamed samples. Mann-Whitney *U* test, $^{*}P < .05$. Scale bar: 50 $\mu$m.

neuroplasticity that promotes neuronal hyperexcitability and motor dysfunction following acute gastroenteritis. A deeper understanding of mechanisms that promote and maintain glial hyperactivity holds great promise for identifying new therapies to improve gastrointestinal dysfunction driven by inflammation in common diseases such as IBD and IBS.

# Methods

## Study Design

The main objective of this study was to investigate the mechanisms responsible for driving and maintaining abnormal enteric circuit activity and motor function following acute intestinal inflammation. In this context, we evaluated whether changes in glia sustain the effects of inflammation on neuronal activity within motility neurocircuits to promote abnormal motility. To achieve this, we used a mouse model of DNBS-induced colitis, which is a well-characterized preclinical method for studying enteric neuroplasticity.[72] Colitis was induced in *Wnt1*$^{Cre2;GCaMP5g\text{-}tdT}$;*GFAP-hM3Dq* female and male mice under isoflurane anesthesia by an 0.1 mL intrarectal enema of 5 mg of DNBS dissolved in 50% ethanol (referred to as post-DNBS group). Control mice received 0.1 mL of 0.9% saline enema (referred to as healthy group). Inflammation in DNBS model peaks between days 2 and 3 and resolves by day 7, which was considered as the endpoint for studying enteric neuroplasticity in the resolution phase of inflammation. Mice were monitored daily, and body weight was recorded to assess disease progression. To evaluate the general sign of distress, disease activity index was daily scored based on weight loss, presence of fecal blood and/or diarrhea, and general behavior. The presence of subclinical inflammation and nitrergic neuron degeneration were assessed by histological damage score and mean packing density of HuC/D and nNOS neurons prior to the colitis induction, at 48 hours after DNBS treatment (the peak of inflammation), and 7 days post-DNBS (the resolution of the inflammation). To explore changes in cellular activity in enteric motor neurocircuits and gut motor function following colitis, colons were collected for ex vivo experiments on day 7 post-DNBS treatment. Calcium ($Ca^{2+}$) imaging was performed using whole-mount preparations of myenteric plexuses to study the activity of enteric neurons and glia that express the genetically encoded $Ca^{2+}$ indicator GCaMP5g and the tdTomato reporter. Neuronal activity was evoked by stimulating the synaptically connected descending, ascending, and circumferantial pathways travelling across the myenteric ganglia by directional FTS. We used chemogenetics to selectively stimulate glial Gq signaling by focal CNO (provided by National Institute on Drug Abuse Supply Program [NDSP]; Division of Therapeutics and Medical Consequences; batch ID 13626-120) application in the same myenteric ganglia. To determine whether motor defects persist after inflammation resolved and investigate the impact of glial hyperexcitability on gut motor function, CMCs were recorded. To further explore the mechanisms driving inflammation-induced glial hyperexcitability, $Ca^{2+}$ imaging recordings were performed in the presence of NO donor, soluble cGMP analog, or EP3 and EP4 receptor antagonists. The study design accounted for sex as a biological variable. $Ca^{2+}$ response magnitude and the number of responding neurons and glia were compared between healthy and post-DNBS groups in both sexes. Additionally, glial permeability assay was conducted. Sample sizes were determined based on previous $Ca^{2+}$ imaging and molecular data published by our laboratories and similar studies described in the literature. The biological replicate number is specified in the figure legends.

## Animals

All animal experiments were conducted in accordance with the National Institutes of Health (NIH) Guide for Care and Use of Laboratory Animals, ARRIVE guidelines and was approved by the Institutional Animal Care and Use Committee (IACUC) at Michigan State University (AUF# PROTO202400108). Male and female mice with C57BL/6 background were used between 10 and 14 weeks of age for all experiments. All mice were maintained on a 12-hour:12-hour light-dark cycle in a temperature-controlled environment with access to food (Diet Number 2919; Envigo) and water ad libitum. Mice expressing the genetically encoded $Ca^{2+}$ sensor GCaMP5g in enteric neurons and glia were generated as previously described.[21] Briefly, B6;129S6-Polr2a$^{Tn(pb\text{-}CAG\text{-}GCaMP5g,\text{-}tdTomato)Tvrd}$/J mice (The Jackson Laboratory, stock no. 024477; RRID: IMSR_JAX:024477) were crossed with B6.Cg-E2f1$^{Tg(Wnt1\text{-}cre)2Sor}$/J mice (The Jackson Laboratory, stock no. 022501; RRID: IMSR_JAX:022501) to generate the offspring herein referred to as *Wnt1*$^{Cre2;}$*GCaMP5g-tdT* mice. This line was crossed with *GFAP::hM3Dq*+/− mice (gift from Ken McCarthy, University of North Carolina at Chapel Hill; RRID: MMRRC_042286-UNC) to generate triple-transgenic *Wnt1*$^{Cre2;GCaMP5g\text{-}tdT}$;*GFAP::hM3Dq* mice. Genotyping was performed by Transnetyx.

## Disease Activity Index

The disease activity index was used to evaluate experimental colitis induction and progression. The cumulative index was determined by scoring daily changes in body weight (0 = none; 1 = 1%–5%; 2 = 5%–10%; 3 =10%–20%; 4 = >20%), stool consistency and occult bleeding (0 = normal; 1 = soft pellets; 2 = pastry and semiformed pellets; 3 = watery pellets containing abundant mucus; 4 = macroscopic blood), and animal behavior and appearance (0 = normal; 1 = coarse hair; 2 = coarse hair and abnormal activity; 3 = markedly hyporesponsive), starting from the day before the DNBS treatment until day 7 when mice were euthanized.

## Colonic Motor Complexes

Colonic motility was assessed in response to colitis ex vivo in *GFAP::hM3Dq* mice as described elsewhere.[35] Briefly, whole intact colons were collected in warmed drug-free Dulbecco's Modified Eagle Medium (DMEM)/F-12, and luminal contents were gently flushed. Oral and aboral ends were secured with surgical silk after being mounted on a stainless-steel rod. Force transducers (Grass Instruments) were connected to the gut wall via surgical silk

approximately 2 cm apart. Tissue was placed into a bath containing DMEM/F12 media (37°C; 11039; Gibco) and adjusted to an initial tension of 0.5 g. Spontaneous CMC production was recorded in LabChart 8 (ADInstruments) for a period of 20 minutes before experiments were conducted. CMCs were defined as a complex in which contraction occurs first at the oral site followed by a contraction at the aboral site. The last 5 minutes of this acclimatization period was used as baseline. 10 $\mu$M CNO was bath applied, and CMCs were recorded for an additional 5-minute interval. Resultant changes in CMC amplitude, integral, frequency, and propagation velocity were calculated in relation to baseline healthy controls.

## Histological Damage Score

Colons were fixed for 48 hours in Carnoy's fixative and stored in 30% ethanol until use. Hematoxylin and eosin (H&E) staining was performed on paraffin-embedded 7-$\mu$m cross-sections of the distal and proximal colon by the Investigative Histopathology Laboratory at MSU. Histological damage was assessed as previously described at distinct time points: prior to colitis induction (pre-inflammation), at 48 hours after DNBS treatment (peak of inflammation), and 7 days after colitis (post-DNBS), to evaluate the degree of inflammation and recovery. The scores was assessed by recording the individual score of (a) distortion and loss of crypt architecture (normal to severe, 0–3), (b) infiltration of inflammatory cells (normal to dense infiltration, 0–3), (c) muscle thickening (presence of marked muscle thickening, 0–3), (d) goblet cell depletion (absence versus presence, 0–1), and (e) crypt abscess (absence versus presence, 0–1).[73] The histological damage is expressed as an average combined score for each group.

## Circular Muscle Myenteric Plexus Whole-mount Preparation

Colons were immediately removed from euthanized $Wnt1^{Cre2;GCaMP5g\text{-}tdT}$;*GFAP::hM3Dq* mice and placed in ice-cold Kreb's buffer consisting of (in mM): 121 NaCl, 5.9 KCl, 2.5 CaCl2, 1.2 MgCl2, 1.2 NaH2PO4, 10 HEPES, 21.2 NaHCO3, 1 pyruvic acid, and 8 glucose (pH adjusted to 7.4 with NaOH). The full-thickness tissues were then opened along the mesenteric border and pinned flat with mucosa facing up in Sylgard-coated Petri dishes. The mucosa was removed by cutting at the level of the lamina propria while separating the layers with forceps. Proximal and distal sections of the colon were then separated and flipped, and the longitudinal muscle and serosa were removed by microdissection to obtain live whole mounts with intact myenteric plexus lying atop the preparation.

## Immunohistochemistry

Longitudinal muscle myenteric plexus (LMMP) whole-mount preparations from segments of healthy and post-DNBS colons were fixed in 4% paraformaldehyde (PFA; 158127; Sigma) for 30 minutes at 4°C and processed for immunohistochemistry (IHC). Briefly, LMMPs were rinsed 3 times (10 minutes each) in phosphate buffered saline (PBS) (3828-01; Avantor) containing 0.1% Triton X-100 (T-PBS; 100032242276; Sigma) followed by a 45-minute incubation in blocking solution (containing 4% normal donkey serum, 017-000-121, Jackson ImmunoResearch; 0.4% Triton X-100; 1% bovine serum albumin in PBS 1X, 001-000-162, Jackson ImmunoResearch) at room temperature. Preparations were incubated with primary antibodies overnight at 4°C and with secondary antibodies for 2 hours at room temperature before mounting (Table 3). Confocal imaging of myenteric ganglia were acquired using an upright Nikon C2 confocal microscope (Nikon Corporation). DAPI was excited using a 405-nm laser, its emission of light was filtered using a 438/24-nm emission filter, and blue was designated as the color assignment in the LUT. The nNOS was excited using a 488-nm laser, its emission of light was filtered using a 525/50-nm emission filter, and green was designated as the color assignment in the LUT. The HuC/D fluorochrome was excited using a 561-nm laser, its emission of light was filtered using a 600/50-nm emission filter, and red was designated as the color assignment in the LUT. Immunofluorescence labeling was observed using 10× and 20× objective lenses (n.a. 0.75, Plan Fluor; Nikon) of an upright epifluorescence microscope (Nikon Eclipse Ni) with a Retiga 2000R camera (Qimaging) controlled by MetaMorph software (v.7.10.1.161, Molecular Devices). An overlay image as well as images of fluorochrome labeling in separate channels were obtained post-acquisition for analysis. Final images were transferred to Adobe Photoshop 2021 (Adobe Systems) for the construction of figure sets. Acquisition parameters were optimized to each tissue as the fluorescence intensity of each probe differed between tissues.

## Focal Tract Stimulation

FTS was used to stimulate interganglionic myenteric nerve bundles in experiments designed to investigate the effects of ascending, descending, and circumferential synaptic pathways activation on enteric motor neurocircuits.

**Table 3.** Primary and Secondary Antibodies Used for Immunofluorescence Labeling

| Antigen | Host | Dilution | Source | Cat# / RRID |
|---|---|---|---|---|
| nNOS | Rabbit | 1:50 | Invitrogen | AB_2313734 |
| HuC/D | Mouse | 1:200 | Invitrogen | AB_2535822 |
| Anti-mouse IgG2b Alexa 594 | Goat | 1:400 | Jackson | AB_ RRID:AB_2338887 |
| Anti-rabbit Alexa 488 | Donkey | 1:400 | Jackson | AB_2313584 |

A custom-assembled tungsten bipolar electrode (World Precision Instruments Inc) was placed on an interganglionic nerve bundle located immediately oral, aboral or lateral to the field of view (FOV) containing the ganglion of interest. The distinct orientation of oral and aboral segments allowed the stimulator to be precisely positioned in proximal and distal regions flanking the FOV. Stimulation was performed using 1-second depolarizing pulses generated by a GRASS S9E Electrical Stimulator with parameters set to 70 V, 10 Hz, and 0.1 ms duration.

## Focal CNO Application

Filamented borosilicate glass microelectrodes were produced using a P-87 Flaming-Brown Micropipette Puller (Sutter Instruments Corporation) and subsequently backfilled with Kreb's buffer containing CNO (100 $\mu$M). Using gentle positive pressure applied via a 1-mL syringe attached to a pipette holder, CNO was puffed onto the surface of the ganglia to evoke glial responses. This technique enables the delivery of drug-containing solution in picoliter volumes, facilitating the study of responses across multiple ganglia within a single preparation. Given the mechanosensitivity of certain enteric neurons, we verified that fluid ejection alone did not activate neurons or glia in myenteric ganglia, consistent with prior observations.[21] It is worth noting that higher drug concentrations were required for this approach compared with bath application experiments, owing to dilution within the bath.

## $Ca^{2+}$ Imaging

Live whole mount circular muscle myenteric plexus (CMMP) preparations from *Wnt1*$^{Cre2;GCaMP5g\text{-}tdT}$*;GFAP::hM3Dq* mice were incubated in DMEM for 45 minutes at 37°C before starting experiments. Preparations were continually perfused with prewarmed (37°C) Kreb's buffer at a flow rate of 2 to 3 mL min$^{-1}$. Myenteric ganglia were visualized through a 20× wide-field water-immersion objective lens (Olympus XLUMPLFLN20xW, 1.0 numerical aperture) on an upright Olympus BX51WI fixed-stage microscope. Ganglia were identified based on their plexiform appearance and high expression of the fluorescent tdTomato reporter in resident glial cells (Figure 3*B–C*). GCaMP5g fluorescence was excited by light passed through a 485-nm/20-nm bandpass filter and detected by reflected light passing through a 515-nm long-pass filter. The tdT fluorescence was excited by light passing through a 535-nm/20-nm bandpass filter and detected by reflected light passing through a 610-nm/75-nm bandpass emission filter. Images of GCaMP5g fluorescence were acquired at a frame rate of 5 frames/s with a Neo sCMOS camera controlled by MetaMorph software (Molecular Devices). Images were saved as *.tiff* files, and recordings were exported as *.tiff* stacks for subsequent analysis. Pretreatments by with the NO donor PAPA NONOate; 100 $\mu$M; 15 minutes of incubation) and cell-permeable cGMP analog 8-Bromoguanosine 3′,5′-cyclic monophosphate (8-Br-cGMP; 100 $\mu$M; 15 minutes of incubation) were performed to test whether restoring nitrergic tone constrains glial hyperactivity and the resulting effects on neurons in the post-inflamed tissues. In a separate set of experiments, preparations were incubated for 30 minutes with EP3 receptors antagonist L-798, 106 (10 $\mu$M; 11129, Cayman Chemical) and EP4 receptors antagonist L-161, 982 (50 $\mu$M; 10011565, Cayman Chemical) to block prostaglandin receptors.

## Tissue Movement

Tissue displacement was analyzed as previously described.[74,75] Videos acquired using Metamorph were imported into ImageJ software and position corrected to maintain muscle orientations on both the x and y axes. The software was calibrated to generate measurements considering the distance in pixels from a known distance. Following, a template-matching plugin was applied and the evoked movement at baseline and activity periods were measured. Tissue movement is described in $\mu$m and movement latency in seconds considering the frames/s acquisition.

## Glial Permeability Assay

EtBr dye uptake was used to measure glial Cx43 hemichannel activity as previously described.[23] LMMP whole-mount preparations were dissected and placed in 35-mm$^2$ Sylgard-coated dishes. LMMP were treated with an enzyme mix containing 1 U/mL Dispase (17105-041, Gibco) and 150 U/mL Collagenase Type II (17101-015, Gibco) for 15 minutes at room temperature and washed 3 times. LMMP was repined to warrant tissue fields of view and incubated for 15 minutes to equilibrate. Next, an incubation of 30 minutes at 37°C in a 5% CO2/95% air atmosphere in either Krebs solution (control) or Krebs solution containing the mimetic peptide antagonists for Cx43 (43Gap26, 100 $\mu$M; 62644, Anaspec, Inc.) was performed. After, treatment was removed and the preparations were incubated with EtBr (5 $\mu$M; 15585-011, Invitrogen) in the presence or absence of the CNO (100 $\mu$M) for 10 minutes at 37°C to drive specific enteric glial activation. The tissues were then washed 3 times with fresh Krebs solution. EtBr fluorescence was immediately recorded using an upright Olympus BX51WI fixed-stage microscope equipped with a 40× water-immersion objective (LUMPlan N, 0.8 n.a.) and a light source passing through a 535-nm/20-nm bandpass filter and detected by reflected light passing through a 610-nm/75-nm bandpass emission filter (Sutter). Ganglia were identified based on plexiform appearance and images were obtained using MetaMorph software (Molecular Devices).

## Statistical Analysis

Whole animals or colons were used as individual n values for in vivo analyses and motility assays, respectively. For packing density analysis, Fiji software (NIH) was used to convert images scale from to $\mu$m$^2$ to mm$^2$. HuC/D(+) and nNOS(+) neurons were counted in 5 to 10 ganglia per mouse in both proximal and distal colon. Then, the average values of both HuC/D(+) and nNOS(+) neurons in the post-DNBS mice at the peak and resolution of inflammation were

corrected by the relative average values of HuC/D(+) and nNOS(+) neurons in the healthy mice, respectively, and plotted as percentage of control (neurons $mm^{-2}$). For $Ca^{2+}$ imaging and dye uptake experiments, the n value represented the averaged ganglionic cellular responses from multiple mice. The specific number of cells analyzed for each stimulation condition, intestinal region, and sex is reported in the figure legends. EtBr fluorescence was used to determine the average glial fluorescence values per ganglion, and the dye uptake in DNBS-treated groups was normalized and expressed as a percentage of the healthy control mean. Data were analyzed using Kruskal-Wallis with Dunn's multiple comparisons test. Representative images of myenteric ganglia from $Ca^{2+}$ imaging experiments are z-projections of time series images of myenteric glia and neurons on stimulation with FTS or focal CNO application in which the maximal peak $Ca^{2+}$ response of responsive cells is falsely colored or shown by temporal-color code. Representative $Ca^{2+}$ imaging traces depict the average change in fluorescence over time in enteric glial cells or neurons within a ganglion evoked by FTS and focal CNO application. $Ca^{2+}$ recordings were analyzed using Fiji software (NIH) as described previously.[21] Briefly, videos were background-subtracted and, when necessary, stabilized using the StackReg and TurboReg plugins. The tdT channel image was used to confirm the identity and location of glial cells in all experiments and to generate corresponding regions of interest (ROIs). Thus, the tdT image was band-pass filtered using Fiji's Free Fourier Transform (FFT) function to filter large objects (down to 40 pixels) and small objects (up to 3 pixels), with a 5% directional tolerance allowed. After filtering, image pixel intensities were auto-scaled and saturated according to the internal ImageJ FFT algorithm. The filtered image was then auto-thresholded using the Intermodes threshold algorithm. The binarized image was segmented using ImageJ's watershed spatial separation algorithm for optimal particle detection. This segmentation was carried out using ImageJ's particle autodetection plugin, which detected objects larger than 400 pixels and with circularity values ranging from 0.0 to 1.0. Extra-ganglionic glial ROIs were excluded. Neuronal ROIs were manually selected after excluding auto-generated glial ROIs based on morphology and tdT expression. $Ca^{2+}$ responses were measured and exported to Microsoft Excel. Only cells recorded within the FOV were included in the analysis. For all experiments, approximately 30 to 60 neurons and an equivalent number of glial cells were analyzed per ganglion, with at least 1 to 2 ganglia used per mouse in each recording condition. The number of mice used is also indicated where appropriate in figure captions. Final data values were quantified as the fold-change in mean cellular fluorescence intensity relative to baseline ($\Delta F/F0$) for each individual cell. For population recruitment studies evaluating the proportion of neurons or glia activated by FTS or focal CNO application, a positive response was defined as a peak fluorescence value greater than 3 standard deviations (SDs) above the average baseline $Ca^{2+}$ level for a fixed recording duration. The average number of responding glial and neuronal cells recruited by FTS or focal CNO application was assessed by defining positive recruitment events as those in which the peak $Ca^{2+}$ response exceeded 3 SDs above the baseline and expressed as an average percentage of responsive cells than the total number of glial or neuronal cells within the analyzed ganglion. All experiments were performed with at least 3 biological replicates and at least 3 animals per group. Data were analyzed using 2-way ANOVA, Šídák's multiple comparisons test, unpaired *t*-test, or unpaired Mann-Whitney *U* test in Graphpad 10.1.2 software (Prism) and are presented as mean ± standard error of the mean (SEM) or SD. A *P* value of less than .05 was considered statistically significant. Illustrations were created using BioRender (https://biorender.com/). All authors had access to the study data and had reviewed and approved the final manuscript.

## References


1. Peery AF, Crockett SD, Murphy CC, et al. Burden and cost of gastrointestinal, liver, and pancreatic diseases in the United States: update 2021. Gastroenterology 2022; 162:621–644.
2. Singh R, Zogg H, Ghoshal UC, Ro S. Current treatment options and therapeutic insights for gastrointestinal dysmotility and functional gastrointestinal disorders. Front Pharmacol 2022;13:808195.
3. Bassotti G, Antonelli E, Villanacci V, et al. Abnormal gut motility in inflammatory bowel disease: an update. Tech Coloproctol 2020;24:275–282.
4. Grover M, Herfarth H, Drossman DA. The functional-organic dichotomy: postinfectious irritable bowel syndrome and inflammatory bowel disease-irritable bowel syndrome. Clin Gastroenterol Hepatol 2009;7:48–53.
5. Keohane J, O'Mahony C, O'Mahony L, et al. Irritable bowel syndrome-type symptoms in patients with inflammatory bowel disease: a real association or reflection of occult inflammation? Am J Gastroenterol 2010; 105(1788):1789–1794; quiz: 1795.
6. Klem F, Wadhwa A, Prokop LJ, et al. Prevalence, risk factors, and outcomes of irritable bowel syndrome after infectious enteritis: a systematic review and meta-analysis. Gastroenterology 2017;152:1042–1054.e1.
7. Halpin SJ, Ford AC. Prevalence of symptoms meeting criteria for irritable bowel syndrome in inflammatory bowel disease: systematic review and meta-analysis. Am J Gastroenterol 2012;107:1474–1482.
8. Ozer M, Bengi G, Colak R, et al. Prevalence of irritable bowel syndrome-like symptoms using Rome IV criteria in patients with inactive inflammatory bowel disease and relation with quality of life. Medicine (Baltimore) 2020;99: e20067.
9. Ahmed M, Pu A, Jencks K, et al. Predictors of irritable bowel syndrome-like symptoms in quiescent inflammatory bowel disease. Neurogastroenterol Motil 2024;36: e14809.
10. Sharkey KA, Mawe GM. The enteric nervous system. Physiol Rev 2023;103:1487–1564.
11. Linden DR, Sharkey KA, Mawe GM. Enhanced excitability of myenteric AH neurones in the inflamed guinea-pig distal colon. J Physiol 2003;547:589–601.

12. Linden DR, Sharkey KA, Ho W, Mawe GM. Cyclooxygenase-2 contributes to dysmotility and enhanced excitability of myenteric AH neurones in the inflamed guinea pig distal colon. J Physiol 2004;557:191–205.
13. Krauter EM, Strong DS, Brooks EM, et al. Changes in colonic motility and the electrophysiological properties of myenteric neurons persist following recovery from trinitrobenzene sulfonic acid colitis in the guinea pig. Neurogastroenterol Motil 2007;19:990–1000.
14. Strong DS, Krauter EM, Mawe GM. From molecules to motion: altering neuronal ion channel function can lead to changes in intestinal motility. Neurogastroenterol Motil 2007;19:329–332.
15. Lomax AE, Mawe GM, Sharkey KA. Synaptic facilitation and enhanced neuronal excitability in the submucosal plexus during experimental colitis in guinea-pig. J Physiol 2005;564:863–875.
16. Hons IM, Storr MA, Mackie K, et al. Plasticity of mouse enteric synapses mediated through endocannabinoid and purinergic signaling. Neurogastroenterol Motil 2012; 24:e113–e124.
17. Roberts JA, Lukewich MK, Sharkey KA, et al. The roles of purinergic signaling during gastrointestinal inflammation. Curr Opin Pharmacol 2012;12:659–666.
18. Linden DR, Couvrette JM, Ciolino A, et al. Indiscriminate loss of myenteric neurones in the TNBS-inflamed guinea-pig distal colon. Neurogastroenterol Motil 2005; 17:751–760.
19. Gulbransen BD, Bashashati M, Hirota SA, et al. Activation of neuronal P2X7 receptor-pannexin-1 mediates death of enteric neurons during colitis. Nat Med 2012; 18:600–604.
20. Seguella L, Gulbransen BD. Enteric glial biology, intercellular signalling and roles in gastrointestinal disease. Nat Rev Gastroenterol Hepatol 2021;18:571–587.
21. Delvalle NM, Dharshika C, Morales-Soto W, et al. Communication between enteric neurons, glia, and nociceptors underlies the effects of tachykinins on neuroinflammation. Cell Mol Gastroenterol Hepatol 2018;6:321–344.
22. Schneider R, Leven P, Glowka T, et al. A novel P2X2-dependent purinergic mechanism of enteric gliosis in intestinal inflammation. EMBO Mol Med 2021;13: e12724.
23. Morales-Soto W, Gonzales J, Jackson WF, Gulbransen BD. Enteric glia promote visceral hypersensitivity during inflammation through intercellular signaling with gut nociceptors. Sci Signal 2023;16: eadg1668.
24. Schneider KM, Blank N, Alvarez Y, et al. The enteric nervous system relays psychological stress to intestinal inflammation. Cell 2023;186:2823–2838.e20.
25. Progatzky F, Shapiro M, Chng SH, et al. Regulation of intestinal immunity and tissue repair by enteric glia. Nature 2021;599:125–130.
26. Brown IAM, McClain JL, Watson RE, et al. Enteric glia mediate neuron death in colitis through purinergic pathways that require connexin-43 and nitric oxide. Cell Mol Gastroenterol Hepatol 2016;2:77–91.
27. Brierley SM, Linden DR. Neuroplasticity and dysfunction after gastrointestinal inflammation. Nat Rev Gastroenterol Hepatol 2014;11:611–627.
28. De Giorgio R, Guerrini S, Barbara G, et al. Inflammatory neuropathies of the enteric nervous system. Gastroenterology 2004;126:1872–1883.
29. Ng QX, Soh AYS, Loke W, et al. The role of inflammation in irritable bowel syndrome (IBS). J Inflamm Res 2018; 11:345–349.
30. Baars JE, Nuij VJAA, Oldenburg B, et al. Majority of patients with inflammatory bowel disease in clinical remission have mucosal inflammation. Inflamm Bowel Dis 2012;18:1634–1640.
31. Spencer NJ, Costa M, Hibberd TJ, Wood JD. Advances in colonic motor complexes in mice. Am J Physiol Gastrointest Liver Physiol 2021;320:G12–G29.
32. Hoffman JM, McKnight ND, Sharkey KA, Mawe GM. The relationship between inflammation-induced neuronal excitability and disrupted motor activity in the guinea pig distal colon. Neurogastroenterol Motil 2011;23, 673–e279.
33. Krauter EM, Linden DR, Sharkey KA, Mawe GM. Synaptic plasticity in myenteric neurons of the guinea-pig distal colon: presynaptic mechanisms of inflammation-induced synaptic facilitation. J Physiol 2007; 581:787–800.
34. Ahmadzai MM, Seguella L, Gulbransen BD. Circuit-specific enteric glia regulate intestinal motor neurocircuits. Proc Natl Acad Sci U S A 2021;118: e2025938118.
35. Ahmadzai MM, McClain JL, Dharshika C, et al. LPAR1 regulates enteric nervous system function through glial signaling and contributes to chronic intestinal pseudoobstruction. J Clin Invest 2022;132:e149464.
36. Chiu IM, Barrett LB, Williams EK, et al. Transcriptional profiling at whole population and single cell levels reveals somatosensory neuron molecular diversity. eLife 2014;3:e04660.
37. Düdükcü Ö, Raj DDA, van de Haar LL, et al. Molecular diversity and migration of GABAergic neurons in the developing ventral midbrain. iScience 2024;27: 111239.
38. Kottick A, Martin CA, Del Negro CA. Fate mapping neurons and glia derived from Dbx1-expressing progenitors in mouse preBötzinger complex. Physiol Rep 2017;5:e13300.
39. Bornstein JC, Furness JB, Smith TK, Trussell DC. Synaptic responses evoked by mechanical stimulation of the mucosa in morphologically characterized myenteric neurons of the guinea-pig ileum. J Neurosci 1991;11:505–518.
40. Erde SM, Sherman D, Gershon MD. Morphology and serotonergic innervation of physiologically identified cells of the guinea pig's myenteric plexus. J Neurosci 1985;5:617–633.
41. Thomasi B, Gulbransen B. Mini-review: intercellular communication between enteric glia and neurons. Neurosci Lett 2023;806:137263.
42. Delvalle NM, Fried DE, Rivera-Lopez G, et al. Cholinergic activation of enteric glia is a physiological mechanism

that contributes to the regulation of gastrointestinal motility. Am J Physiol Gastrointest Liver Physiol 2018; 315:G473–G483.
43. McClain JL, Fried DE, Gulbransen BD. Agonist-evoked Ca2+ signaling in enteric glia drives neural programs that regulate intestinal motility in mice. Cell Mol Gastroenterol Hepatol 2015;1:631–645.
44. McClain J, Grubišić V, Fried D, et al. Ca2+ responses in enteric glia are mediated by connexin-43 hemichannels and modulate colonic transit in mice. Gastroenterology 2014;146:497–507.e1.
45. McClain JL, Gulbransen BD. The acute inhibition of enteric glial metabolism with fluoroacetate alters calcium signaling, hemichannel function, and the expression of key proteins. J Neurophysiol 2017; 117:365–375.
46. Grubišić V, McClain JL, Fried DE, et al. Enteric glia modulate macrophage phenotype and visceral sensitivity following inflammation. Cell Rep 2020;32:108100.
47. Valès S, Bacola G, Biraud M, et al. Tumor cells hijack enteric glia to activate colon cancer stem cells and stimulate tumorigenesis. EBioMedicine 2019;49:172–188.
48. Linden DR. Colitis is associated with a loss of intestinofugal neurons. Am J Physiol Gastrointest Liver Physiol 2012;303:G1096–G1104.
49. Manning BP, Sharkey KA, Mawe GM. Effects of PGE2 in guinea pig colonic myenteric ganglia. Am J Physiol Gastrointest Liver Physiol 2002;283:G1388–G1397.
50. Sofroniew MV. Molecular dissection of reactive astrogliosis and glial scar formation. Trends Neurosci 2009; 32:638–647.
51. Sofroniew MV, Vinters HV. Astrocytes: biology and pathology. Acta Neuropathol 2010;119:7–35.
52. Chao C-C, Gutiérrez-Vázquez C, Rothhammer V, et al. Metabolic control of astrocyte pathogenic activity via cPLA2-MAVS. Cell 2019;179:1483–1498.e22.
53. Burda JE, O'Shea TM, Ao Y, et al. Divergent transcriptional regulation of astrocyte reactivity across disorders. Nature 2022;606:557–564.
54. Mayo L, Trauger SA, Blain M, et al. Regulation of astrocyte activation by glycolipids drives chronic CNS inflammation. Nat Med 2014;20:1147–1156.
55. Sardar D, Cheng Y-T, Woo J, et al. Induction of astrocytic Slc22a3 regulates sensory processing through histone serotonylation. Science 2023;380:eade0027.
56. Lee H-G, Rone JM, Li Z, et al. Disease-associated astrocyte epigenetic memory promotes CNS pathology. Nature 2024;627:865–872.
57. Lee H-G, Wheeler MA, Quintana FJ. Function and therapeutic value of astrocytes in neurological diseases. Nat Rev Drug Discov 2022;21:339–358.
58. Lee H-G, Lee J-H, Flausino LE, Quintana FJ. Neuroinflammation: an astrocyte perspective. Sci Transl Med 2023;15:eadi7828.
59. Heredia DJ, Grainger N, McCann CJ, Smith TK. Insights from a novel model of slow-transit constipation generated by partial outlet obstruction in the murine large intestine. Am J Physiol Gastrointest Liver Physiol 2012; 303:G1004–G1016.
60. Murakami M, Ohta T, Otsuguro K-I, Ito S. Involvement of prostaglandin E(2) derived from enteric glial cells in the action of bradykinin in cultured rat myenteric neurons. Neuroscience 2007;145:642–653.
61. Hennig GW, Gould TW, Koh SD, et al. Use of genetically encoded calcium indicators (GECIs) combined with advanced motion tracking techniques to examine the behavior of neurons and glia in the enteric nervous system of the intact murine colon. Front Cell Neurosci 2015;9:436.
62. Broadhead MJ, Bayguinov PO, Okamoto T, et al. Ca2+ transients in myenteric glial cells during the colonic migrating motor complex in the isolated murine large intestine. J Physiol 2012;590:335–350.
63. Chen G, Park C-K, Xie R-G, et al. Connexin-43 induces chemokine release from spinal cord astrocytes to maintain late-phase neuropathic pain in mice. Brain J Neurol 2014;137:2193–2209.
64. Weiss BE, Kraner SD, Artiushin IA, Norris CM. Elevated calcineurin activity in primary astrocytes leads to the dephosphorylation of connexin 43 in conjunction with increased membrane permeability. Neuroreport 2024; 35:673–678.
65. Retamal MA, Cortés CJ, Reuss L, et al. S-nitrosylation and permeation through connexin 43 hemichannels in astrocytes: induction by oxidant stress and reversal by reducing agents. Proc Natl Acad Sci U S A 2006; 103:4475–4480.
66. Esposito G, Capoccia E, Turco F, et al. Palmitoylethanolamide improves colon inflammation through an enteric glia/toll like receptor 4-dependent PPAR-$\alpha$ activation. Gut 2014;63:1300–1312.
67. De Filippis D, Esposito G, Cirillo C, et al. Cannabidiol reduces intestinal inflammation through the control of neuroimmune axis. PloS One 2011;6:e28159.
68. Costa DVS, Bon-Frauches AC, Silva AMHP, et al. 5-fluorouracil induces enteric neuron death and glial activation during intestinal mucositis via a S100B-RAGE-NF$\kappa$B-dependent pathway. Sci Rep 2019; 9:665.
69. Angelo MF, Aguirre A, Avilés Reyes RX, et al. The proinflammatory RAGE/NF-$\kappa$B pathway is involved in neuronal damage and reactive gliosis in a model of sleep apnea by intermittent hypoxia. PLoS One 2014;9: e107901.
70. van Baarle L, De Simone V, Schneider L, et al. IL-1R signaling drives enteric glia-macrophage interactions in colorectal cancer. Nat Commun 2024;15:6079.
71. Stoffels B, Hupa KJ, Snoek SA, et al. Postoperative ileus involves interleukin-1 receptor signaling in enteric glia. Gastroenterology 2014;146:176–187.e1.
72. Morampudi V, Bhinder G, Wu X, et al. DNBS/TNBS colitis models: providing insights into inflammatory bowel disease and effects of dietary fat. J Vis Exp 2014: e51297.
73. Li R, Kim M-H, Sandhu AK, et al. Muscadine grape (Vitis rotundifolia) or wine phytochemicals reduce intestinal inflammation in mice with dextran sulfate sodium-induced colitis. J Agric Food Chem 2017;65:769–776.

74. Smith-Edwards KM, Najjar SA, Edwards BS, et al. Extrinsic primary afferent neurons link visceral pain to colon motility through a spinal reflex in mice. Gastroenterology 2019;157:522–536.e2.
75. Nestor-Kalinoski A, Smith-Edwards KM, Meerschaert K, et al. Unique neural circuit connectivity of mouse proximal, middle, and distal colon defines regional colonic motor patterns. Cell Mol Gastroenterol Hepatol 2022;13:309–337.e3.

**Received January 9, 2025. Accepted September 17, 2025.**

**Correspondence**
Address correspondence to: Brian D. Gulbransen, PhD, Department of Physiology, Michigan State University, 567 Wilson Road, East Lansing, Michigan 48824. e-mail: gulbrans@msu.edu; tel: (517) 884-5121.

**CRediT Authorship Contributions**
Luisa Seguella, PhD (Data curation: Lead; Formal analysis: Equal; Investigation: Lead; Project administration: Equal; Supervision: Equal; Writing – original draft: Equal)
Beatriz Thomasi, PhD (Data curation: Lead; Formal analysis: Equal; Investigation: Equal; Writing – original draft: Supporting)
Silvia Basili Franzin (Formal analysis: Supporting; Investigation: Supporting)
Jonathon L. McClain, MS (Formal analysis: Supporting; Investigation: Supporting)
Rafaella Lavalle (Formal analysis: Supporting)
Aurora Zilli (Data curation: Supporting; Formal analysis: Supporting; Investigation: Supporting; Methodology: Supporting)
Visha Parmar (Investigation: Supporting)
Giuseppe Esposito, PhD (Supervision: Supporting)
Brian Gulbransen, PhD (Conceptualization: Lead; Data curation: Equal; Funding acquisition: Lead; Project administration: Lead; Supervision: Lead; Validation: Lead; Visualization: Lead; Writing – original draft: Lead)

**Conflicts of interest**
The authors disclose no conflicts.

**Funding**
Brian D. Gulbransen receives support from grants R01DK103723 and R01DK120862 from the National Institute of Diabetes and Digestive and Kidney Diseases of the National Institutes of Health. The content is solely the responsibility of the authors and does not necessarily represent the official views of the National Institutes of Health.

**Data Availability**
The datasets used and/or analyzed during the current study are available from the corresponding author on reasonable request. The methods and study materials used in the current study are fully described in the Methods section of the manuscript.